

COMPUTATIONAL ANALYSIS OF THE RESPONSE OF BURIED STEEL  
PIPELINES DUE TO SUDDEN GROUND MOTION

by

Kshitij P. Gawande

A thesis submitted to the faculty of  
The University of North Carolina at Charlotte  
in partial fulfillment of the requirements  
for the degree of Master of Science in  
Mechanical Engineering

Charlotte

2015

Approved by:

---

Dr. Harish P. Cherukuri

---

Dr. Ronald E. Smelser

---

Dr. Vincent Ogunro

© 2015  
Kshitij P. Gawande  
ALL RIGHTS RESERVED

## ABSTRACT

KSHITIJ P. GAWANDE. Computational analysis of the response of buried steel pipelines due to sudden ground motion.

(Under the direction of DR. HARISH P. CHERUKURI)

Pipeline systems are the primary means by which natural gas and liquid fuels are distributed to delivery points from pumping and compressor stations. Many of these pipelines are buried underground and consequently are susceptible to sudden ground motions resulting from seismic events such as earthquakes and landslides. Damage sustained by the pipelines during such events, if severe, can lead to disruptions in the fuel supplies and significant economic losses.

The objective of this numerical study is to model and analyze the response of a buried pipeline in a strike-slip fault movement. Considering large deformations in the pipeline, a completely nonlinear finite element analysis is carried out using ABAQUS/Explicit. During any ground motion, the pipelines may be subject to one or all of axial, bending and shear-type of loads. These loads can lead to large compressive stresses which, in turn, can lead to local and/or global buckling failure. In the present work, the interaction of the pipeline with the surrounding soil due to sudden ground movement is studied by taking into account the contact between the pipeline and the soil, the nonlinear response of soil, the nonlinear material material response and geometric nonlinearities. The onset of buckling mode failure in the pipeline is studied as different parameters are varied. Specifically, the pipe diameter-to-thickness ratio, the internal pressure, the fault displacement and fault offset rates are varied to better understand the pipeline response due to seismic loads. Based on these studies, conclusions are drawn concerning the allowable internal pressures and diameter-to-thickness ratios for the fault displacements and fault-offset rates that this work and

the previously published literature considered.

## DEDICATION

I would like to dedicate my thesis to my loving parents, Surekha and Prashant Gawande, my brother Utkarsh, my mentor Dr. Harish Cherukuri and all my friends.

## ACKNOWLEDGMENTS

I would like to express the deepest appreciation to my advisor and mentor, Dr. Harish Cherukuri, for his continuous encouragement and unconditional support. He provided me the opportunity to freely choose my path, while sharing his invaluable experience and knowledge as well as his precious time. Without his guidance and persistent help, this project could have not been completed.

I would also like to express my sincere appreciation to Dr. Ronald E. Smelser and Dr. Vincent Ogunro for graciously accepting to serve on my thesis committee.

I offer my enduring gratitude to the department of Mechanical Engineering and Engineering Science, faculty and staff, as well as Mr. Jonathan Halter and Mosaic Computing. During the research program, I was grateful to get assistance from some of my fellow students and research group, this includes Apurva Joshi, Chinmay Avachat and Mandar Vaidya. Finally, I would like to thank all my roommates and friends for always being there for me.

## TABLE OF CONTENTS

CHAPTER 1: INTRODUCTION	1
1.1 Background	1
1.2 Faults	3
1.2.1 Normal Fault	5
1.2.2 Reverse Fault	5
1.2.3 Strike-Slip Fault	6
1.2.4 Oblique-Slip Fault	6
1.3 Geological Background	6
1.4 Thesis Organization	9
CHAPTER 2: LITERATURE REVIEW	10
2.1 Previous Research	10
2.2 Buckling	14
2.3 Guidelines for Pipe Design	16
CHAPTER 3: OBJECTIVES AND NUMERICAL MODELING	18
3.1 Objectives	18
3.2 Case I: Pipe Without the Soil	18
3.3 Case II: Pipe-Soil Model	19
3.3.1 Finite Element Analysis Approach	21
3.4 Material Modeling	23
3.4.1 Modeling of Pipe Using Conventional Shell Elements	26
3.5 Contact and Loads	26
3.6 Meshing Techniques	27
3.7 Parametric Study	29
CHAPTER 4: RESULTS AND DISCUSSIONS	32

	viii
4.1 Case I: Pipe Without the Soil	32
4.1.1 Mesh Refinement	35
4.1.2 Standard Dimension Ratio	35
4.1.3 Internal Pressure	37
4.2 Case II: Pipe-Soil Model	38
4.2.1 Mesh Refinement	45
4.2.2 Standard Dimension Ratio	45
4.2.3 Fault Offset Rate	46
4.2.4 Internal Pressure	48
CHAPTER 5: SUMMARY AND CONCLUSIONS	51
5.1 Recommendations for Future Work	53
REFERENCES	54

## LIST OF FIGURES

FIGURE 1.1: 78 inches wide and 0.7 inches thick pipe bent in Chi-Chi earthquake. [4].	2
FIGURE 1.2: The San Andreas fault [5].	4
FIGURE 1.3: Normal fault [9].	5
FIGURE 1.4: Reverse fault [9].	6
FIGURE 1.5: Strike-slip fault [10].	7
FIGURE 1.6: Oblique-slip fault [11].	7
FIGURE 3.1: An idealized model (without the soil) for studying the onset of buckling in pipes. The effect of the soil on the pipe is modeled as an external pressure.	19
FIGURE 3.2: A schematic of the pipe-soil system. The inset shows a cross-section of the system.	20
FIGURE 3.3: Top view of the pipe-soil system. Schematics of both the undeformed and deformed configurations are shown.	21
FIGURE 3.4: Stress-strain curve of API X65 steel [27].	23
FIGURE 3.5: Mohr-Coulomb yield surface in $\sigma - \tau$ stress space [33].	25
FIGURE 3.6: Boundary conditions for the model: the bottom face (highlighted in red) is constrained in Y-direction.	27
FIGURE 3.7: Boundary conditions for the model: the surfaces highlighted in red are constrained in X and Z-directions. Note that the right-most face consists of both the soil and pipe cross-sections.	28
FIGURE 3.8: A finite element mesh for the soil block. A fine mesh is used in the fault-plane zone. The left and right blocks are partitioned into two blocks each for better mesh control. The element type used for meshing is the 8-node reduce integration brick element (C3D8R in ABAQUS).	29

- FIGURE 3.9: An example of the mesh used for the pipe model. The element type is the 4-node conventional shell element with reduced integration (S4R in ABAQUS). 30
- FIGURE 4.1: The contours represent the axial strains in the deformed pipe with buckling due to external pressure. 32
- FIGURE 4.2: The contours represent axial strains before buckling in the pipe. The wavy pattern depicts wrinkling pattern in the shell mode of buckling. 33
- FIGURE 4.3: The contours represent axial strains after buckling in the pipe. The central region shows tension-compression-tension buckling failure. 33
- FIGURE 4.4: Evolution of axial strains in the buckled region of the pipe. 34
- FIGURE 4.5: Axial stresses on the two integration points of the shell element in the buckled region of the pipe. 35
- FIGURE 4.6: Axial strains on the two integration points of the shell element in the buckled region of the pipe. 36
- FIGURE 4.7: The contours represents axial strains in the pipe after buckling (at 0.3 seconds). 1,2,3 and 4 shows the increasing number of elements and the respective buckling patterns. 36
- FIGURE 4.8: Standard dimension ratio vs time of buckling. 37
- FIGURE 4.9: bulging shape buckling in a pipe with an internal pressure. 38
- FIGURE 4.10: Effect of internal pressure on time of buckling. 39
- FIGURE 4.11: Deformation of the pipe-soil system. The contour colors represent the displacement component (in meters) in X-direction. 40
- FIGURE 4.12: Anti-symmetrically deformed pipe with an inset showing the deformed regions. The contours colors represent axial strains. 40
- FIGURE 4.13: The contours represent axial strains in the pipe; a) Wrinkling pattern before buckling, b) Shell mode buckling. 41
- FIGURE 4.14: Evolution of axial strains in a buckled region of the stationary block. 41

FIGURE 4.15: Time history of axial strains on the two integration points of the shell element in the pipe (region A).	42
FIGURE 4.16: Time history of axial stresses on the two integration points of the shell element in the pipe (region A).	43
FIGURE 4.17: Time history of hoop stresses on the two integration points of the shell element in the pipe (region A).	44
FIGURE 4.18: Evolution of axial strains in a tension region of the stationary block.	44
FIGURE 4.19: Different mesh refinements in the pipe and respective buckling patterns.	45
FIGURE 4.20: Effect of standard dimension ratio on the critical fault displacement.	47
FIGURE 4.21: A diamond shaped buckling.	47
FIGURE 4.22: Effect of fault offset rate on critical fault displacement.	48
FIGURE 4.23: Effect of fault offset rate on the time of buckling.	49
FIGURE 4.24: Buckling pattern in pipe with an internal pressure in a pipe-soil model.	49
FIGURE 4.25: Effect of an internal pressure on the critical fault displacement.	50

## TABLE OF CONTENTS

TABLE 3.1: Parameters for defining the inelastic response of API X65 steel. For points a,b and c, see Figure 3.4.	24
TABLE 3.2: Material properties of the idealized soil material.	24
TABLE 4.1: Comparison of results with and without mass scaling.	45
TABLE 4.2: Effect of mesh refinement on the pipe response.	46

## CHAPTER 1: INTRODUCTION

### 1.1 Background

Vast networks of pipelines are used onshore and offshore globally to transmit oil, gas and water. Considering the safety of the society, pipes are generally installed underground; however, there may be exceptions. The distance of the source and the delivery station can vary from a few meters to thousands of miles. Therefore, the pipelines are often exposed to severe weather conditions, natural calamities and several other forces. To illustrate, temperature can vary from sub-zero temperatures to over 100° F; earth strata can be rock solid or cohesion-less sand, and loads experienced can be external pressures from vehicles, bridges, structures and soil. In addition, pipelines can undergo landslides, earthquakes, permanent ground deformation, fault movement and liquefaction of soil. Stringent rules for designing and maintenance of pipelines have been developed to ensure pipeline integrity and safety [1].

There have been numerous incidents where pipelines have experienced failure due to sudden ground motion, which interrupted their functioning. In Japan's Miyagiken-Oki earthquake [29] thousands of people were without water for days because of 350 breaks at different positions in the pipeline. In 1971, San Fernando Earthquakes, there were 450 breaks in an underground water pipeline and 52 breaks in a span of 6 miles of a transmission pipeline and numerous buckled portions as well. Moreover, the damages in oil and gas pipelines can lead to severe fatalities and huge economic loss. In Batesville/Panola, Mississippi, there was a damage in a natural gas pipeline due to failure of the repair sleeve installed over a wrinkle bend. This led to fire and a total repair cost of \$734,698 [2]. From February 2011 to June 2012, there have been

8 incidents in just gas transmission pipelines due to earth movement in the United States with total damages at a cost of over 7 million dollars [3]. This clearly shows that there is a need to improve the design of pipes and make them more safer.



Figure 1.1: 78 inches wide and 0.7 inches thick pipe bent in Chi-Chi earthquake. [4].

Sudden earth movements occur because of faults created during earthquakes. An understanding of fault mechanics, fault types and the reason for the occurrences of fault motions are essential to be better equipped to design buried pipelines and handle potential damage to them. The fault is created by the sudden movement of tectonic plates relative to each other with the release of a huge potential energy from the earth's crust. This sudden release of energy is what creates earthquakes. This will be explained briefly in the next section. There are a few faults which are continuously moving and are called active faults. The prime example is the San Andreas fault. A part of southern California is moving in a North West direction and the prediction is that it will merge with Alaska in the next 50 million years. This active fault is moving with the speed of 22 mm per year, and there are more active faults present in the other parts of the world such as Turkey, Switzerland etc. For a pipeline that is crossing an active fault, there is an obvious chance that it would fail due to fault

motion. During the Chi-Chii earthquake in 1999, many pipelines sustained significant damage. In Figure 1.1, a bent piece of a water pipe (2 meters long and 0.7 inches thick) is shown. As can be seen from this figure, the major damage seems to be due to buckling.

In the fault movement, the pipeline quickly becomes inelastic due to the large deformations involved. From reviews and case studies, it has been proven that every case is different depending on the pipe material, thickness, diameter, internal pressure, soil condition, the magnitude of the earthquake, fault type and fault length. The different failure types are wrinkling, local buckling, failure in tension and failure in bending. For understanding such a complex behavior of pipes, analytical methods are not adequate. Hence, the present study employs the finite element method to study the response of pipelines to sudden ground movement.

To understand the integrity of pipelines due to sudden ground motion, numerous research studies were carried out in past 50 years. Initially, scientists used analytical approaches and recently researchers began using numerical or computational approaches. Depending on the mechanisms, ASME has designed rules and codes for maintaining the integrity of pipelines. A brief explanation of all the methods and approaches in the previous and current research is summarized in the next chapter.

## 1.2 Faults

A fault is a fracture of the earth's crust generated by the relative movement of tectonic plates. The pressure and the friction deep in the plates prevent it from moving or sliding with each other. As a result, stresses develop for years, decades or even centuries. When the critical stress is reached, a sudden slip occurs followed by the huge sliding of plates. This sudden release of potential energy causes shaking of the ground and is called an earthquake. The higher the stresses, the higher will be the magnitude of an earthquake.

To understand faults more clearly, US Geological Survey [6] gives a very nice

analogy with finger snapping. The fault can be very easily understood with a snap of our fingers. Press your thumb and a middle finger on each other and apply force sideways as well. As you push your fingers on each other, friction gets generated, and friction is preventing the fingers from sliding. When the stress value overcomes the friction, you get an audible response because of sudden release of energy. A similar process occurs in an actual fault. Here, the tectonic plates slide as stresses in the earth's crust overcome the friction between the plates. A huge amount of energy is released by this sliding which creates a P-type wave.



Figure 1.2: The San Andreas fault [5].

Faults occur in three steps: start of the sliding of plates, growth of the fault length, and stoppage of fault growth. According to van der Elst [7], plates are continuously growing, consequently changing their boundaries. The continuous growth leads to a bending of a fault or it can give rise to more faults. The generation of a fault and the earthquake is not a smooth event; it occurs in a series of jerks. Once a fault is created, it is very probable that an earthquake will occur on that same fault in a 'stric-slip' mode, instead of creating a new one. Stric is the moment of 'no slip' while slip creates an earthquake, combined it is called a 'stric-slip' fault. The length of the fault may

or may not increase depending on the magnitude of the earthquake. Also, the length of a fault can vary from few meters to a hundreds of miles.

Mainly, there are two types of faults, active faults and inactive faults. In an active fault, the plates are continuously moving, and in an inactive fault, the plates come to a complete halt after the slip event. There is still a possibility of becoming reactivated because of the earth stresses. Based on the relative movement of the tectonic plates, the faults are categorized in four types:

### 1.2.1 Normal Fault

A normal fault occurs where the crust is being pulled apart, and the block above the fault (hanging wall block) moves downwards with respect to block below the fault (footwall block) [8]. This type of fault can also be categorized as dip-slip fault or gravity fault. Whenever the main sense of the fault is vertical, it is called as dip-slip fault. e.g. Sierra Nevada/Owens Valley.

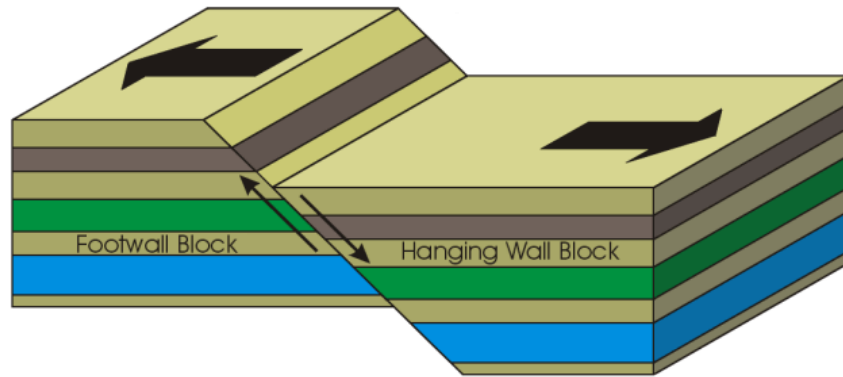


Figure 1.3: Normal fault [9].

### 1.2.2 Reverse Fault

A reverse fault occurs in the collision zones of plates and is due to compression forces of the crust. The block above the fault (hanging wall block) moves up with respect to the block below the fault (footwall block). This can also be categorized as dip fault or thrust fault. The live examples are the Himalayas and Rocky Mountains.

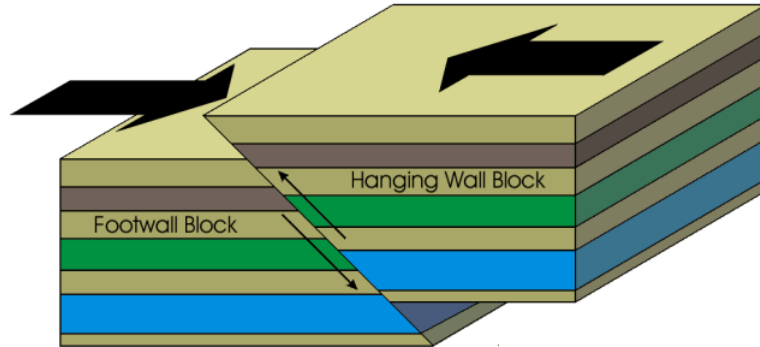


Figure 1.4: Reverse fault [9].

### 1.2.3 Strike-Slip Fault

In a strike-slip fault, the tectonic plates move horizontally to each other with no or very little vertical movement. This fault is caused by the shear forces of the plates. This can be sub-categorized in left-lateral and right lateral strike-slip faults depending on the direction of the movement. The prime example is the San Andreas fault in California. This fault creates a vertical fault plane. In our study, this is an important fault because all the previous research has proved that this fault causes the highest damage to the pipelines compared to other faults.

### 1.2.4 Oblique-Slip Fault

When a dip-slip fault and a strike-slip fault occur together, it creates an oblique-slip fault. Therefore, the faults explained earlier are the basic faults and a combination of any of those can be called as an oblique-slip fault. However, every fault can have both the components, vertical and horizontal, but to consider it as an oblique fault, both components must be significant.

## 1.3 Geological Background

This section briefly gives the commonly used geological terms, and they will be used for the rest of this thesis.

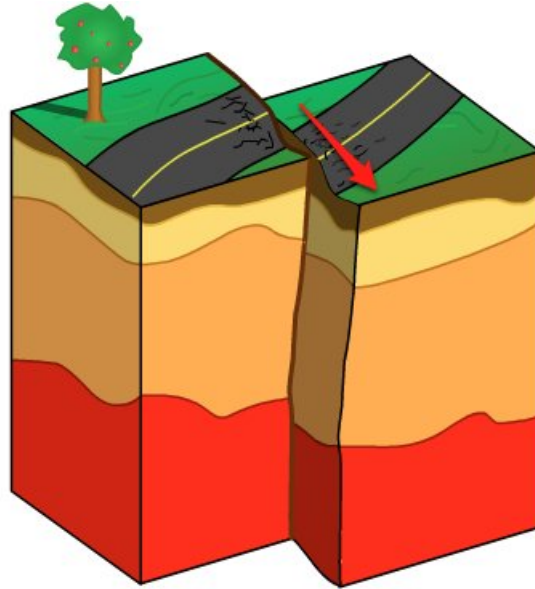


Figure 1.5: Strike-slip fault [10].

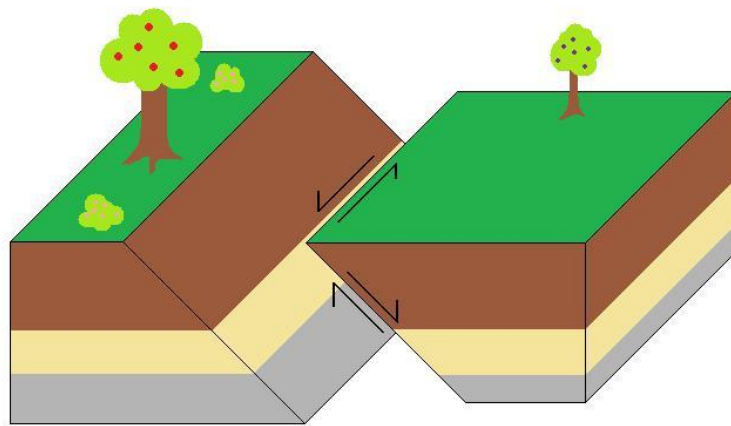


Figure 1.6: Oblique-slip fault [11].

### 1. Rupture Speed

Rupture speed is the speed at which rupture front moves across the fault surface. It can be as high as the velocity of stresses in that region, but this speed is found typically to be less than shear wave speed. According to Andrea Bizzari [12], the rupture speed is linearly proportional to the peak ground speed.

### 2. Slip Velocity

The velocity at which active faults are moving continuously, in other words, the rate at which tectonic plates are moving relative to each other is termed as the slip velocity. The slip velocity can vary from a few millimeters per year to a few centimeters per year. The San Andreas fault is moving with the velocity of  $22\pm-1$  mm/year.

### 3. Fault Displacement

The relative displacement caused due to the tensile or the compressive forces in the crust that moves the plates in the opposite direction relative to each other; this is called as fault displacement. One can confuse fault displacement with fault length; both are different. The displacement can vary from a few millimeters to few meters while the length can be from few millimeters to hundreds of miles.

### 4. Peak Ground Velocity (PGV)

In the case of moderate to strong earthquakes, spectrometer overwhelms but the velocity pattern clearly depicts earthquake pattern. Peak ground velocity can be defined as the maximum velocity experienced by the particle on the earth's surface. This quantity can be a very good correlation or index factor for the designing of tall and flexible structures. The maximum value recorded for PGV is 183 cm/s according to US Geological Survey [13] in the 1994 Northridge earthquake. However, in the study from McGarr and Fletcher, the maximum PGV used is 4.7 m/s recorded in the Chi-Chi earthquake [14].

### 5. Fault Plane

The relative displacement in the tectonic plates creates a plane which is termed as a 'Fault Plane'. The angle of this plane is a deciding factor in a normal fault and a reverse fault. The Fault plane is almost perpendicular in the strike-slip fault.

## 1.4 Thesis Organization

This chapter introduced the motivation behind this research and the necessity for the improvement in the pipe design. Also, it explains the geological background which is important to consider in the next chapters of this thesis.

The next chapter will summarize the relevant previous research carried out in this field. It will also point out the inconsistencies in different studies as well as flaws in them, and will direct the current research.

The third chapter has the objective of this thesis in explaining the methodology. This chapter also explains the detailed modeling and different cases considered. Furthermore, the advantages and disadvantages will be stated for different FEA approaches.

The Results and Discussion will critique the results and also present a parametric study to examine the effect of various parameters on the response of a buried pipeline.

Finally, the Summary and Conclusion of the study will contain the questions posed by this study and possible improvements in the present design. Also, future work will be recommended based on the results and simplifications of this study.

## CHAPTER 2: LITERATURE REVIEW

### 2.1 Previous Research

The pipeline response depends on the magnitude of an earthquake, the nature of the fault, the speed and length of the fault, and topographic conditions of the affected region [15]. There have been a significant number of experimental, numerical and analytical studies to capture the response of pipelines. The subsequent paragraphs briefly elaborate the relevant research and findings.

Newmark and Hall [16] conducted the first work on this topic, and they studied the mechanical response of buried pipelines under strike slip fault displacement. The objective was to study the fault carrying capability of pipe buried at different depths with different pipe materials and thicknesses. The applied fault displacement was more than 10 feet. A simplified analytical technique was adopted assuming the pipe was a long cable. In this method, the resistance offered by the pipe to the slip was directly related to the angle of friction and geostatic pressure. They concluded that smaller frictional force, lower grades of steel, and greater thickness of pipe achieve better resistance. The study also commented on the depth of cover and the survival limit for different grades of pipe with the varying thickness.

This study was further improved by Kennedy et al. [17]. They concentrated on shallow buried pipelines with larger horizontal and vertical fault displacements. There were some improvements in their analytical approach such as nonuniform friction assumed between the pipe and the soil as opposed to uniform friction in the previous study [16]. They concluded that the presence of internal pressure increases the bending strains and negligibly changes the axial strains. Also, a change in pipe diameter has

insignificant effect on axial strains. This study also concluded that a larger diameter to thickness ratio reduces the fault carrying capability and the capability increases with higher crossing angles. Further, work by Wang and Yeh [18] improved these results by including the bending stiffness of the pipe material. They studied shallow buried pipelines and concluded that larger crossing angles, smaller buried depths, smaller pipe diameters and smaller friction angles are the favorable characteristics for pipe capability. The results of this study were compared to the Kennedy et al. results and agreed with it. In spite of these improvements, the analytical method was not very accurate because of its simplifications. In another study by Wang and Wang [19], a cantilever beam analogy was used to analyze buried pipelines in the fault movement. They concluded that the effect of soil pipe friction angle has a significant effect on pipeline response.

Takada et al. [20] made the first attempt to use the finite element method for analyzing the pipeline response. They improved the previous models by using a beam-shell hybrid model for the pipe. The objective was to develop a simplified model to obtain the maximum strain in the pipes undergoing fault movement. Prior to their work, no one appears to have taken the pipe cross-section into account explicitly since the previous studies were based on cable models. Moreover, the study presented a general formula for maximum tensile strain, and it also states that bending angles are more important than the crossing angles for maximum strains in steel pipes.

Karamitros et al. [21] proceeded with an analytical method but with several improvements in the previous methods, including a beam-on-elastic foundation and elastic beam theory. These models were used to obtain axial and bending strains in the pipeline. The authors reviewed the previous work and made modifications such as using a bi-linear stress strain curve to consider the nonlinearity of the material. Also, this method is capable of analyzing the curved part of the pipe and the stress distribution on the pipeline cross-section. This method was verified using finite element

methods but a very coarse finite element model was used.

More recently, Liu et al. [22] studied pipelines under fault crossings. The study focused on the effects of material properties, wall thickness, and relation between maximum strain and fault angle. A numerical simulation was performed with hybrid shell-beam elements for the pipe similar to Karamitros et al. [21]. Again, the finite element model was performed with a coarse mesh and with large fault displacements. This study concluded that the effect of vertical fault displacement is independent of the intersection angle. It also concluded that larger intersection angles exhibit failure in bending mode while lower intersection angle shows failure in a tensile mode. Furthermore, the authors state that, in the presence of internal pressure, maximum tensile strain reduces at lower intersection angles and increases at higher intersection angles. Recently, Nadukuru et al. [23] analyzed three finite element models of buried concrete pipelines and concentrated on the reaction forces at the end of the pipe. These results were verified by experiments done at Cornell University. These finite element models were built with a bell and spigot joint which makes it more realistic. To reduce the computational time for the simulation, the offset rate used was 1 meter per 3 seconds, However, the offset rate of an actual incident was given as 1 foot per 60 seconds. Both studies used hexahedral elements for their numerical models. However, their analyses did not capture buckling modes of failure. Therefore, a drawback of these two studies is that if buckling modes are not captured and occur before weld failure, onset of failure may be predicted to occur much later than they actually occur.

In the series of papers, Abdoun et al. [24] [25] [26] performed centrifuge tests on high density polyethylene (HDPE) pipeline experiencing a fault. The objective was to study the effect of soil moisture content, fault offset rate, burial depth and pipe diameter. The paper concluded that offset rates do not influence the pipe behavior and peak strains, but it also states that higher offset rates give higher bending strains. As the burial depth increases, pipe stiffness and consequently the strains also increase.

In another study with Da Ha et al. [25] [26] he has investigated the effects of pipe fault orientation on axial and bending stresses. And they found that axial stresses are highly influenced by the fault angle whereas changes in bending stresses are insignificant. This paper also talks about the transverse force-deformation relation and shows that it varies along the length of a pipe. This strain data was verified with the commonly used Kennedy model and similar trend of strain evolution was recorded but with the low peaks of strain magnitudes. Moreover, Abdoun et al. also studied the normal fault and stated that the deformation occurring in normal fault is asymmetric as opposed to anti-symmetric deformation in the case of strike slip fault. In all the experimental studies, extrapolation has been used to obtain data for the actual models, but the reliability of extrapolated results in nonlinear behavior is questionable.

On the other hand O'Rourke et al. [31] studied the large scale model of HDPE pipeline crossing the fault using special split box design with a very systematic approach to experiment. In this study, a log spiral model was used to obtain the horizontal component of force on the pipe. Another objective of this research was to improve the water supply system of the Los Angeles Department of Water and Power. The numerical model was designed but not much information or results were provided as this study was more focused on experiments. In summary, the findings are: 1) the lateral force on the pipe is measured almost same in 3D and 2D tests, 2) the lateral force on the pipe is almost the same whether dry sand or partially saturated sand is used.

Vazouras et al. [27] carried out a thorough finite element study on a buried steel pipeline crossing an active fault. This study considered quasistatic strike-slip fault acting on a pipe in a normal direction and mainly focused on strain development in the pipe. Parametric study of diameter to thickness ratio, fault displacements, width of fault slip zones was included in this study. Also, study of the effect of internal pressure, material hardening, different pipe and soil material and mode of failure

was incorporated. This study concluded that fault carrying capacity: increases with decreasing diameter to thickness ratio, and decreases slightly with increasing internal pressure. And fault width and material hardening does not have significant effect on the fault carrying capacity of pipe. Importantly, this paper successfully captured the buckling mode failure in the pipe. This paper also commented that pipe soil friction coefficient does not have significant effects on numerical results, which clearly contradicts the results of Wang and Wang [19]. In a subsequent paper, Vazouras et al. [28] studied the response of steel pipelines crossing a fault at an angle and concluded that increase in fault crossing angle favors the fault carrying capacity of pipe.

Meanwhile, excellent reviews were written in this field and few of them are summarized here. Liang et al. [29] has covered almost all of the work done till then and convincingly pointed out that buried pipelines get damaged due to permanent ground deformation instead of wave propagation. However, there are few cases where pipelines get damaged due to wave propagation, and it is when the pipeline is closer to the epicenter and the amplitude of the wave is very high. The author has also deduced that site conditions such as non-uniformity of soil and hilly topographic regions lead to more damage to the pipelines. Furthermore, damage severity of the pipelines was also shown with ample examples which clearly state the need for more research in this field. Besides, Datta [30] has investigated the evolution of study of seismic analysis and behavior of buried pipelines. He has pointed out the numerical difficulties of the problem which explains the high degree of simplification in all the studies until then. This paper excellently suggests the future scope for improvements in modeling pipe-soil interactions.

## 2.2 Buckling

The most prevalent modes of failure in pipe are bending mode failure and tension mode failure. In this study, higher fault crossing angles are assumed, and since it has been shown by the previous studies that for higher crossing angles, the bending mode

is dominating, buckling failure due to bending forces is explained here.

Buckling is a failure mode in which high compressive load causes a sudden failure of a structural member in a sideways direction. Mathematically, it is a failure mode in which bifurcation occurs at a point and the possibilities are a compressed state or a laterally deformed state. In the case of pipe, buckling is observed usually in two types- beam buckling and shell mode buckling. When a long and small diameter pipe experiences axial compression, it tears up the ground and buckles like a beam, this is called as beam buckling. While in shell type buckling, a large diameter pipe experiencing axial compression and restrained in lateral direction undergoes reduction in axial rigidity and localized buckling occurs.

The shell mode of buckling occurs in a set of steps: The axial compression gives rise to wrinkling pattern followed by increase in amplitude of these wrinkles. After certain increase in the load, one wrinkle will dominate and further proceeds to form a sharp kink or a rupture. Examples of failure modes are formation of a local kink, a diamond shaped buckling and a bulging shaped buckling.

In this defined procedure of localized shell buckling, the point at which structure can be assumed to be failed is not clear and hence, there is a need to define the onset of buckling. There is no exact definition for it. Therefore, many researchers make their own definitions and buckling criteria. For instance, Vazouras et al (2010) [27] assumed that the onset of wrinkling is the point at which pipe starts moving outward in the area of maximum compression, while according to Kyriakides [32], onset of buckling and failure are two different events. Some researchers define the failure criteria by ovalization occurrence in the pipe. In the present study, buckling is assumed to occur when there is local bending, that is, when there are both tensile and compressive stresses locally across a thickness of the pipe. Therefore, we define the onset of buckling to be that time when at some thickness in the pipe, local bending first occurs. In our analyses, we use shell elements to model the pipe. Therefore, we

look for those elements in which local bending first occurs.

### 2.3 Guidelines for Pipe Design

ASME has strict rules for manufacturing, installation and maintenance of the pipelines. This section will explain the common terms, definitions and different design factors related to the pipeline design. Pipeline is not just a pipe carrying fluid, but comprises all the parts through which fluid transfer such as valves, flanges, regulators, compressing units, pressure vessels etc.

Pipes are designed and classified according to the areas where they sit, e.g. deserted land, urban areas, small town etc. There are four Location Classes and accordingly different design factors defined by ASME. A Location Class 1 is any 1 mile area having less than 10 buildings such as wasteland, mountains, farmland, etc. And a Location Class 1 is subdivided into Division 1 and Division 2, and in Division 1, the design factor is in between 0.72 and 0.8 and the pipe is tested for 1.25 times the maximum operation pressure. Division 2 is where the design factor does not cross 0.72 and the pipe is tested successfully for 1.1 times the maximum operation pressure. A Location Class 2 is any 1 mile area with number of buildings from 10 to 46, for e.g. small towns, industrial area etc. A Location Class 3 is any 1 mile area where number of buildings is greater than 46 and consists of shopping center, residential areas, etc. A Location Class 4 is similar to a Location Class 3 but consists of areas with heavy traffic, dense population, multistory buildings, etc.

The pipe distribution system is divided into two types: high pressure distribution system and low pressure distribution system. In a high pressure distribution system, pressure in the main pipe is higher than the delivery pressure of the fluid to the consumer, which is regulated by the valves. In low pressure distribution system, a supplier delivers fluid at the same pressure which is required at the consumer level. The design formula and factors considered for the thickness and the design pressure

of a pipeline is given by Equation 3.4,

$$P = \frac{2 \times S \times t}{D} \times F \times E \times T \quad (2.1)$$

where,  $P$ = Design pressure,  $S$ = Specified minimum yield strength (SMYS),  $D$ = Nominal outside diameter,  $F$ = Design factor,  $E$ = Longitudinal joint factor,  $t$ = Thickness, and  $T$ =Temperature derating factor.

Moreover, for the installation of pipelines, depth of cover i.e. buried depth is also specified according to Location Classes and nominal pipe size (NPS). It varies from 12 to 36 inches depending on the diameter and a Location Class. Specified minimum yield strength (SMYS), a commonly used term in design parameters, is the yield strength expressed in pounds per square inch and is the minimum yield strength prescribed by the specification under which pipe is purchased from the manufacturer. One more important definition is the standard dimension ratio, which is the ratio of outer diameter to the thickness of the pipe.

## CHAPTER 3: OBJECTIVES AND NUMERICAL MODELING

### 3.1 Objectives

The objective of this study is to analyze and understand the response of a typical pipeline due to sudden ground movement using the Finite Element Method. This study focuses on the role of various parameters such as the internal pressure, diameter-to-thickness ratio and fault offset rate on the pipe deformation. Moreover, the present study concentrates on the onset of buckling and different buckling patterns in the pipelines as the fault offset rate and applied displacements are varied. Considering the complexity due to nonlinearity of the soil-pipe interaction, the analysis will be divided into two steps: Case I- modeling of pipe without the soil and Case II- modeling of pipe-soil assembly. The commercial finite element software, ABAQUS/Explicit 6.13 is used for modeling and postprocessing as well. In the next two sections, the two cases and the proposed models along with the material models are discussed. It is hoped that these cases will provide insight into the physics of the deformation of pipe and will eventually lead to an efficient design.

### 3.2 Case I: Pipe Without the Soil

In case I, we consider only the pipe without the soil with the purpose being to understand the buckling mode of deformation of the pipe as various parameters and external loads are applied. The simpler model also allows for the mesh-size requirements for accurate prediction of the onset of buckling and buckling patterns.

The pipe is taken to be 60 meters in length and 0.914 meters in diameter. The load applied is similar to the type of load that a buried pipe is expected to experience due to sudden ground motion. The pipe is divided into two parts of equal lengths.

On one part, an external pressure is applied on half the surface. On the second part, an equal pressure is applied on the other half of the surface as shown in Figure 3.1. The pipe is fixed on the right end and the left face is traction free.

Since the pipe is thin-walled, shell elements are appropriate for the finite element model. The specific element type used is the S4R element which is a four-noded element with reduced integration.

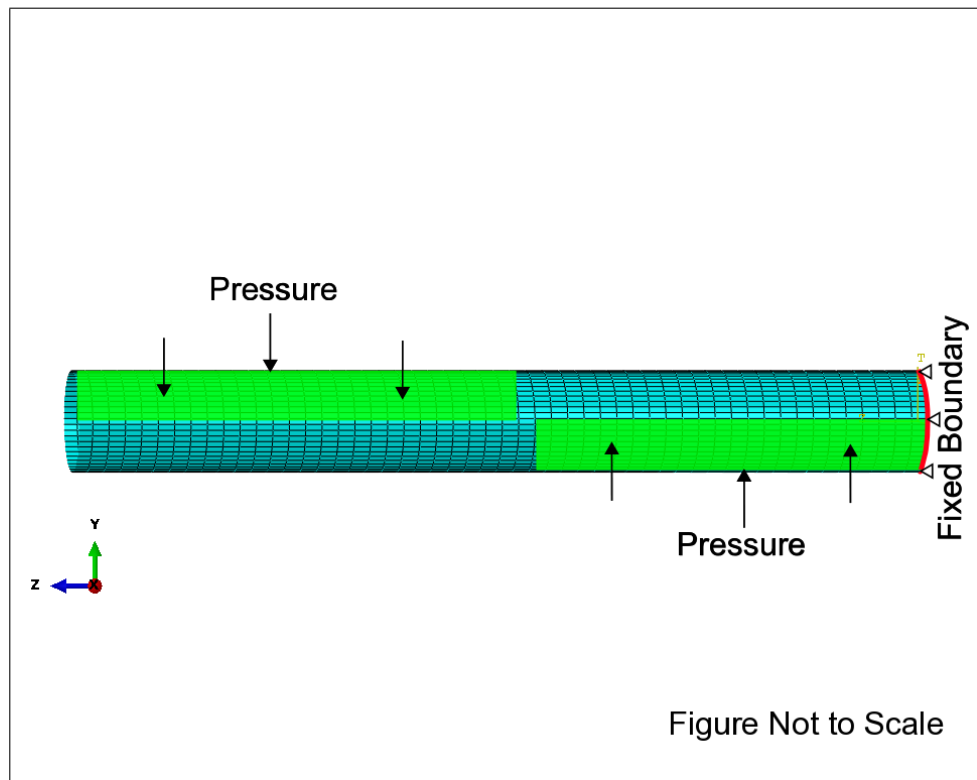


Figure 3.1: An idealized model (without the soil) for studying the onset of buckling in pipes. The effect of the soil on the pipe is modeled as an external pressure.

### 3.3 Case II: Pipe-Soil Model

In case II, we consider that a buried pipe. The soil surrounding the pipe is taken to be rectangular with dimensions of  $10 \text{ m} \times 5 \text{ m} \times 60$ . The pipe is again taken to be  $0.914 \text{ m}$  in diameter and  $60 \text{ m}$  in length. It is buried at a depth of  $2.5 \text{ m}$  in the soil. The pipe-soil system is shown in Figure 3.2. These dimensions are similar to those considered by Newmark and Hall [16] and Vazouras et. al (2010) [27].

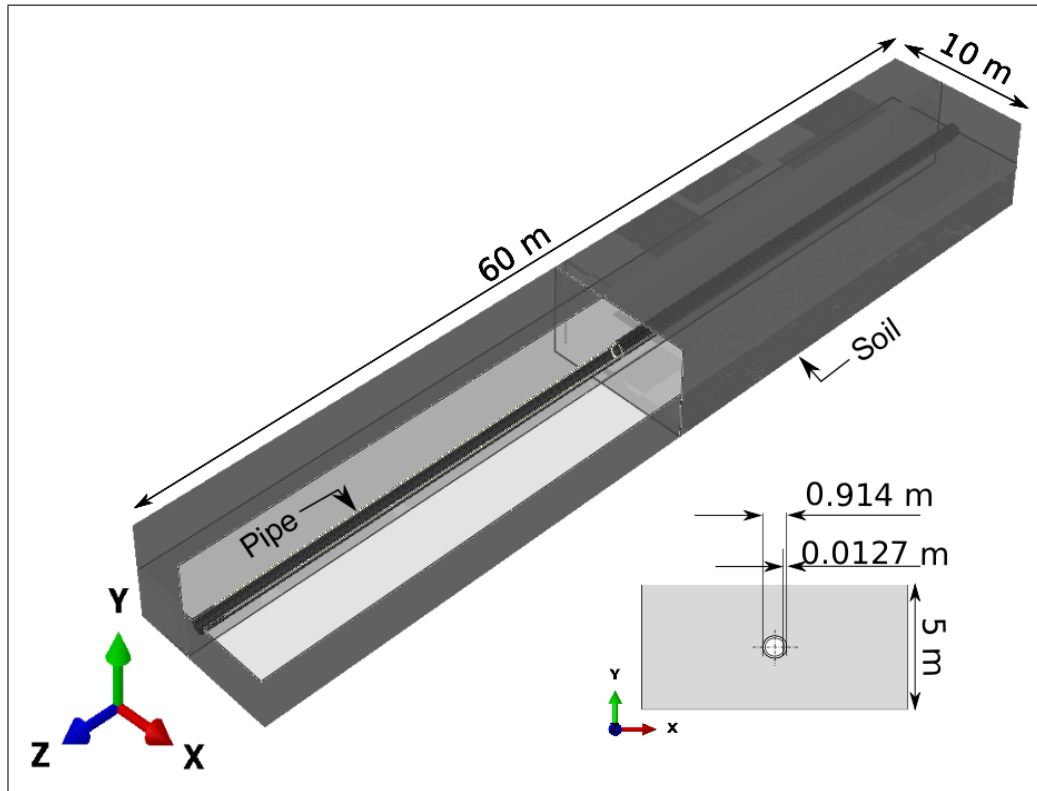


Figure 3.2: A schematic of the pipe-soil system. The inset shows a cross-section of the system.

The deformation of the pipe and soil due to fault motion is modeled as follows. The soil-pipe system is broken up into three blocks: a moving block (M), a fault-slip width block and a stationary block (S) as shown in Figure 3.3. The block on the left (M) experiences a movement due to the strike-slip fault while the block on the right is stationary. The arrows represent the direction of fault motion. Due to this motion, a narrow region between the M and S blocks undergoes severe deformation. This deformation is accommodated by considering a finite width fault-slip width block. In the present studies, this width is taken to be 0.33 m. A previous parametric study by Vazouras et al. [27] shows that the magnitude of this width does not have significant effect on the pipe response.

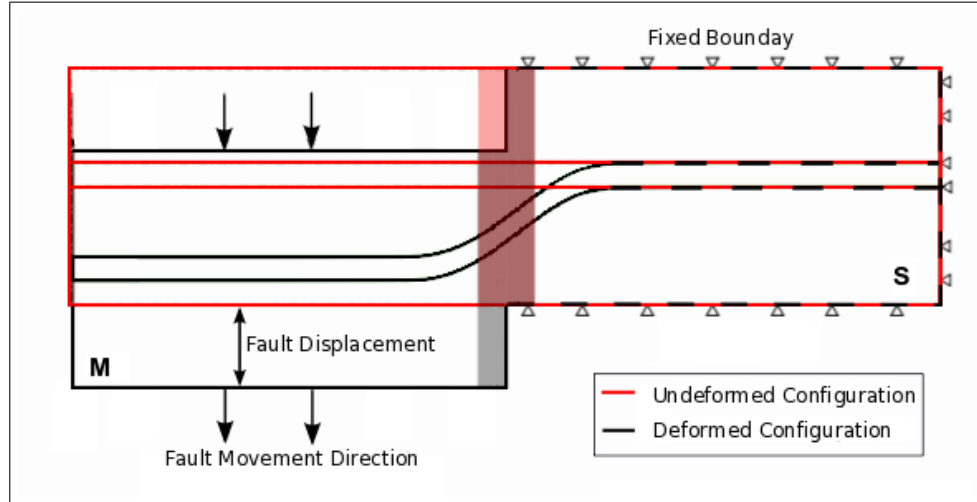


Figure 3.3: Top view of the pipe-soil system. Schematics of both the undeformed and deformed configurations are shown.

### 3.3.1 Finite Element Analysis Approach

The solution to any finite element analysis problem can be approached by an explicit or an implicit algorithm. The implicit algorithms are ideally suited for quasi-static problems and problems where dynamic effects are not important. Explicit methods are used for analyzing dynamic problems where inertial effects are important.

In an actual pipe-soil model, soil always experiences geostatic force. Therefore, to employ this in the numerical model, analysis will be carried out in two steps: gravity analysis and fault movement analysis. Since gravity analysis is a quasistatic process, implicit algorithm is the appropriate method to solve it. However, the fault movement is a sudden process, hence, implicit algorithm may or may not be capable of capturing its physics. An attempt to use the implicit methods for both the steps did not lead to buckling deformations as have been observed in previous studies. Therefore, the explicit method was used for solving both the steps.

Implicit methods have the advantage that they are unconditionally stable. Explicit methods on the other hand are conditionally stable. The time-step cannot be arbitrarily specified and is limited by the largest natural frequency that the finite

element mesh can resolve [34]. The constraint on the time step is given by

$$\Delta t \leq \frac{2}{\omega_{max}}, \quad (3.1)$$

where  $\omega_{max}$  is the maximum frequency that the mesh can resolve. In terms of the dilatational wavespeed  $c_d$ , the time increment  $\Delta t$  can be estimated as

$$\Delta t \approx \frac{L_{min}}{c_d} \text{ with } c_d = \sqrt{\frac{\lambda + 2\mu}{\rho}}. \quad (3.2)$$

Here,  $L_e$  is a characteristic length of the smallest element present in the model,  $\lambda$  and  $\mu$  are the Lamé parameters and  $\rho$  is the mass density. Thus we note that the time increment  $\Delta t$  is inversely proportional to the square root of the density.

In quasistatic processes, the inertial effects are small. When an explicit method is used to solve such problems, since the method is conditionally stable, the time increment is limited by the stability considerations and therefore, even a quasi-static solution can take a long time to obtain. For this reason, mass scaling is often used to increase the time increment. When the density is increased, the dilatational wave speed decreases and therefore the allowable time increment size increases. Mass scaling changes the inertial forces in the problem, which can cause significant change in the solution, and hence the scaling factor has to be chosen such that it does not increase the total kinetic energy significantly.

In the gravity step, the deformation of the pipe due to gravity is concerned. This analysis is a quasistatic process. However, since we are using an explicit approach that uses very small timesteps, the computational time to obtain a solution can be significant. Hence, a global mass scaling is used here with a factor of 50 after a trial and error process. This particular value for mass scaling does not appear to alter the solution significantly. However, it reduces stable time increment from 2.5e-7 to 4.6e-6; a significant savings in computational time.

### 3.4 Material Modeling

The material properties for the pipe and the soil materials are listed below. This section explains material models for modeling the elastic and inelastic behavior of the material.

According to ASME B31.8 [1], there are different grades of pipe material for different operations, different locations and different internal fluids. In this study, a gas pipeline is assumed passing through the Location Class 1, Division 2. A widely used material for this purpose is API X65 grade steel. The Young's modulus and Poisson's ratio for this steel are 210 GPa and 0.3 respectively. The density is 8000 kg/m<sup>3</sup>. The experimental curve is shown in Figure 3.4 (see [27]). For our modeling purposes, the curve is approximated as a perfectly plastic material from a to b and then linearly-hardening from b to c. The data used for this model is shown in Table 3.1. The Mises plasticity theory is used for modeling the elastoplastic behavior of the material.

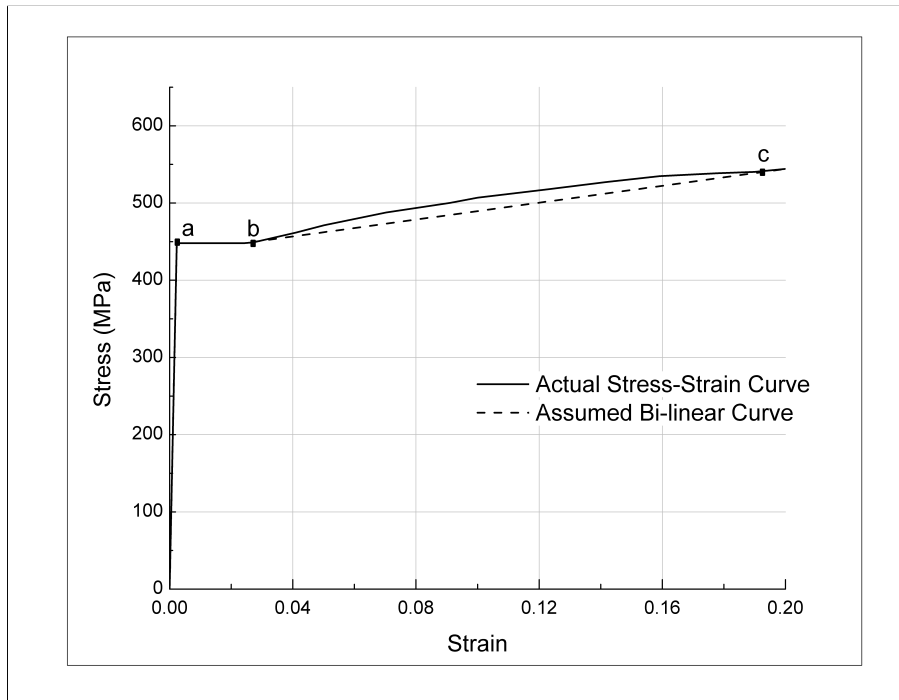


Figure 3.4: Stress-strain curve of API X65 steel [27].

An idealized clay is considered for the soil block. The soil is modeled as a Mohr-

Coulomb material and the cohesivity is taken to be 50 KPa. The rest of the Mohr-Coulomb parameters and other material properties for this material are listed in Table 3.2

Table 3.1: Parameters for defining the inelastic response of API X65 steel. For points a,b and c, see Figure 3.4.

Point	Yield Stress (MPa)	Plastic Strain
a	450	0.0
b	450	0.0279
c	548	0.1679

Table 3.2: Material properties of the idealized soil material.

Density	1800 $kg/m^3$
Young's Modulus	25 $MPa$
Poisson's Ratio	0.5
Cohesion	50 $kPa$
Friction angle	0°
Dilation angle	0°

### Mohr-Coulomb Criterion

Generally, material models used for soil are Mohr-Coulomb and Drucker-Prager material models. We conducted a preliminary study on soil-pipe systems to compare the results from the models. This study led us to conclude that plastic strain evolves

faster in Mohr-Coulomb materials than in Drucker-Prager materials. Therefore, we consider only the Mohr-Coulomb criterion for the rest of the present work.

In 1776, Coulomb gave a failure criterion and in 1900, Mohr stated that failure occurs when Mohr's circle is tangent to the yield surface. There is equivalence between the linear form of Mohr's equation and Coulomb's equation which is given by

$$\tau = c - \sigma_n \tan \phi \quad (3.3)$$

where  $\tau$  = shear strength,  $c$  = cohesion,  $\phi$  = friction angle, and  $\sigma_n$  = normal stress. For elastic behavior, the stress-strain behavior depends on the Young's modulus and the Poisson's ratio while the plastic deformation depends on the friction angle and cohesion in the material. The yield surface in the Haigh-Westergaard space is a cone with the cross-section being an irregular hexagon.

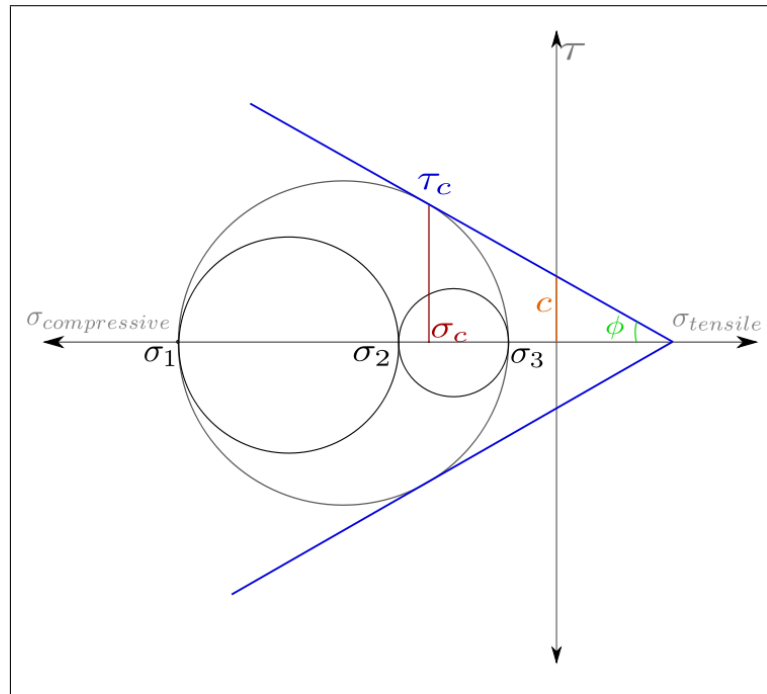


Figure 3.5: Mohr-Coulomb yield surface in  $\sigma - \tau$  stress space [33].

Figure 3.5 shows a Mohr-Coulomb Yield Surface in a  $\sigma - \tau$  space which clearly explains the cohesion ( $c$ ) and angle of friction  $\phi$ . When the angle of friction is zero,

the Mohr-Coulomb criterion will reduce to Tresca criterion. The maximum allowable value for the friction angle is  $\pi/2$ . In this study, the friction angle is taken as zero assuming an idealized clay.

### 3.4.1 Modeling of Pipe Using Conventional Shell Elements

Modeling of shell elements is one the most complex factors in pipe-soil analyses because of the combined nonlinearity of the pipe-soil interaction and the materials. In ABAQUS, cylindrical shell elements have specific orientation and that may or may not be the same as of the whole domain. In order to reorient it, new coordinate system was formed and proper steps were taken according to the ABAQUS manual 6.13 [34]. The normals should be pointing outwards for the smooth running of the contact definitions. Moreover, for maintaining the accuracy of the shell elements, 5 integration points were considered for each element. Also, care is taken while defining the offset definitions of the shell elements. Since the outer diameter of pipe is specified, the top surface should be given the diameter assignments.

## 3.5 Contact and Loads

The contact between the soil and pipe is defined by treating the pipe as the master surface and the soil as the slave surface. Surface to surface contact is modelled in ABAQUS 6.13 and a frictional coefficient ( $\mu$ ) of 0.3 is provided. Since the pipe is discretized using shell elements, care has been taken to make sure that the normals of the shell elements are pointing outward.

To simulate the strike-slip fault in the model, a fault displacement is given to the moving block in the positive X-direction. This fault displacement is applied to all the outer surfaces of the moving block as well as to the end nodes of the pipe. Figure 3.3 shows the movement of the block and the expected shape of the deformed pipe.

To accommodate the stresses due to gravity, we have included gravity analysis before actual fault displacement takes place as explained in Section 3.3.1. And to support

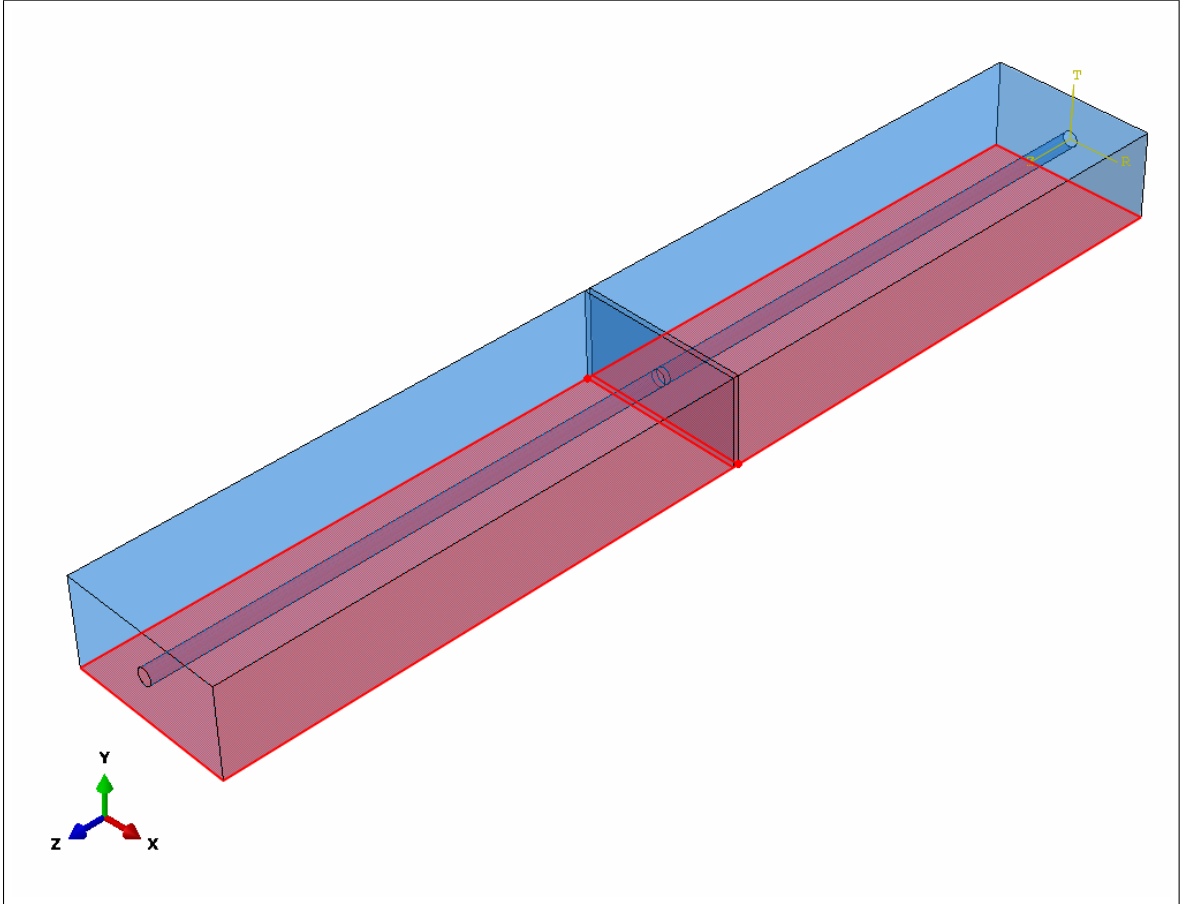


Figure 3.6: Boundary conditions for the model: the bottom face (highlighted in red) is constrained in Y-direction.

this, the displacement of the bottom surface is restrained in the vertical direction as shown in Figure 3.6. While the left block moves forward, the right stationary block is constrained as follows: the displacement of the outer surfaces excluding top and bottom of the stationary block are constrained in X and Z directions as shown in Figure 3.7. This holds the block stationary while allowing for the deformation of the soil inside it.

### 3.6 Meshing Techniques

For meshing the soil block, an eight-node, continuum three dimensional elements with reduced integration (C3D8R) are used. Finer mesh is used near the fault surface while a coarser mesh is used in the other areas as shown in Figure 3.8. A total

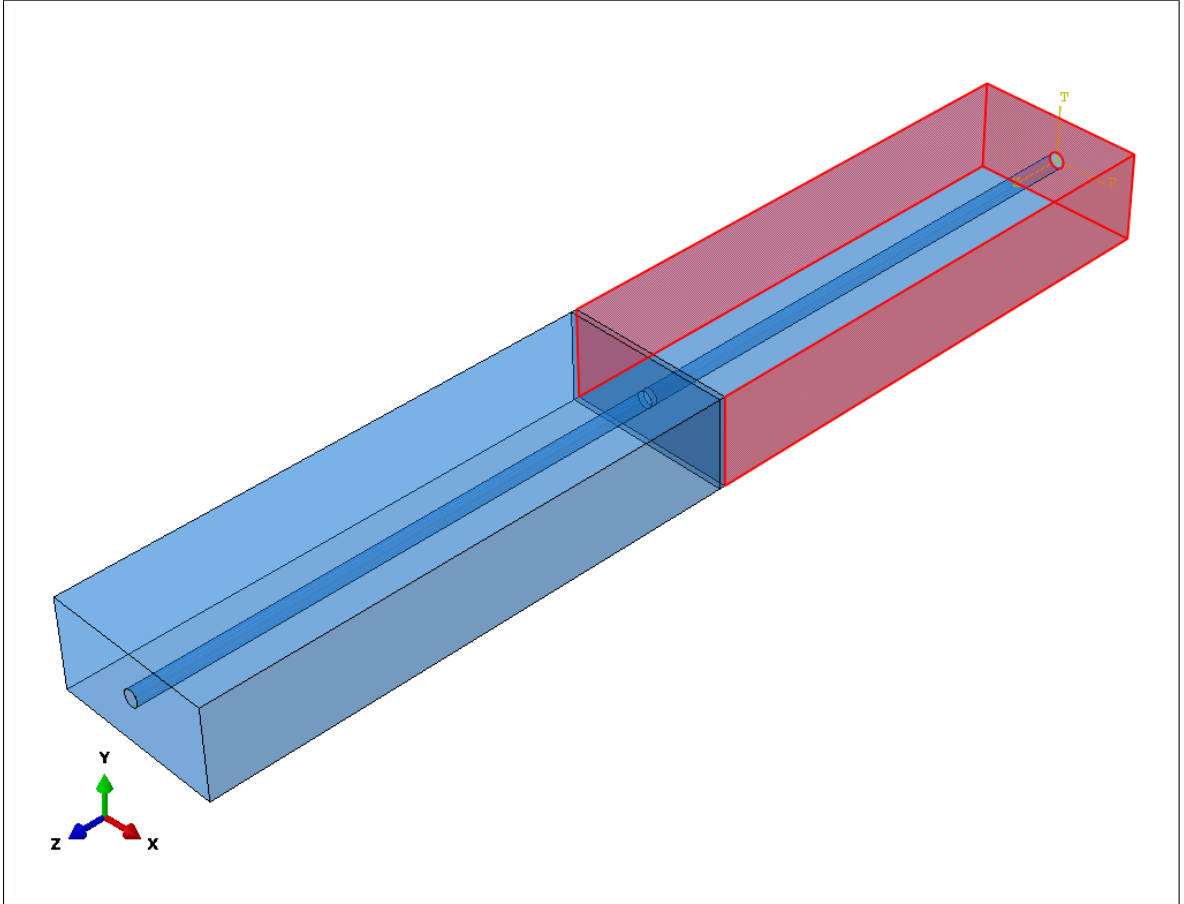


Figure 3.7: Boundary conditions for the model: the surfaces highlighted in red are constrained in X and Z-directions. Note that the right-most face consists of both the soil and pipe cross-sections.

of 62985 elements are created for the soil block. The pipe is modelled with four-node conventional shell elements with reduced integration (S4R) and biased meshing. Approximately, 59 elements around the circumference of the pipe are found to be enough (mesh refinement studies are presented in the next chapter). In all, 99412 elements are generated for the pipe as shown in Figure 3.9. Using shell elements for the pipe allow us to observe the shell mode of buckling and study its evolution. One reason for using conventional shell elements is that contact is on only one side of the shell. On the other hand, continuum elements are more useful for contact on both the sides of the shell. For nonlinear problems FE-formulations overestimated the stiffness of the system. Reduced integration leads to reduced stiffness. For this reason, reduced

integration is used with all the elements.

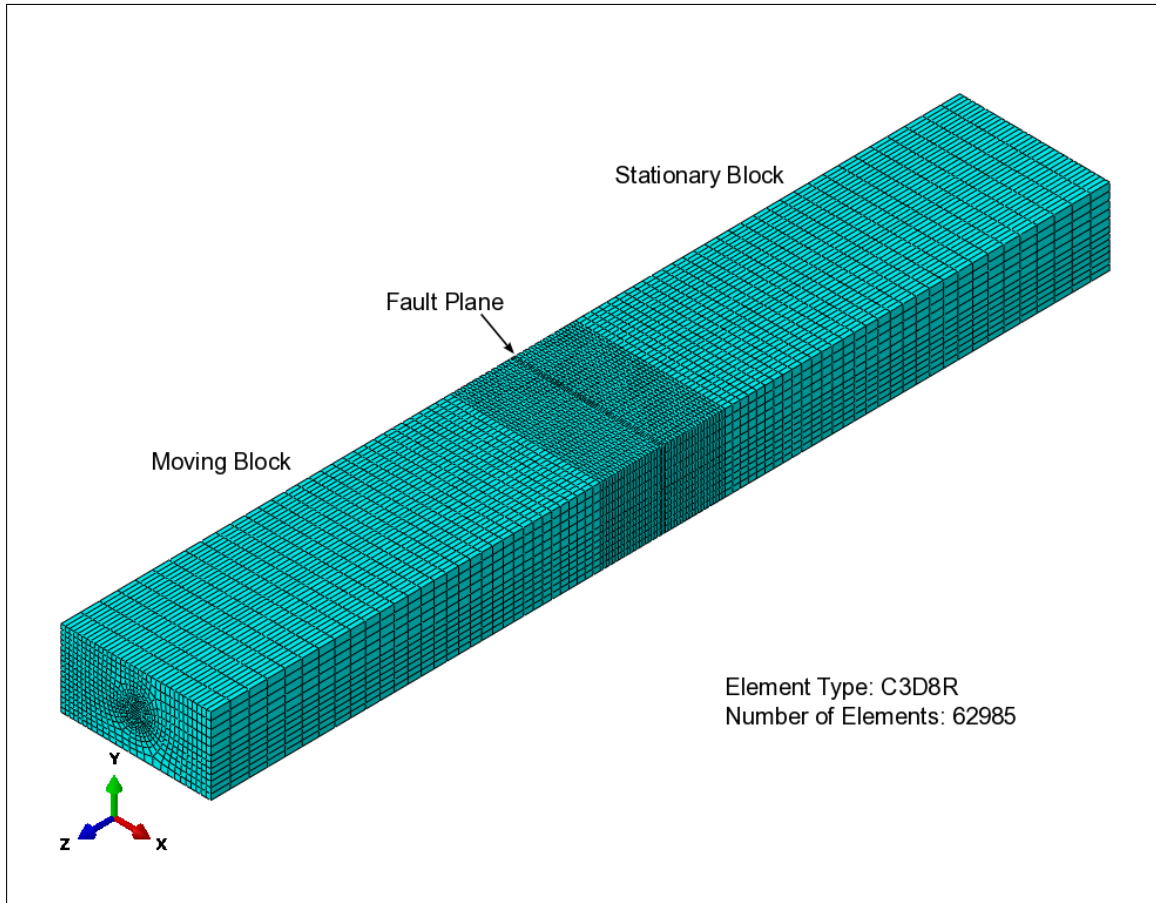


Figure 3.8: A finite element mesh for the soil block. A fine mesh is used in the fault-plane zone. The left and right blocks are partitioned into two blocks each for better mesh control. The element type used for meshing is the 8-node reduce integration brick element (C3D8R in ABAQUS).

### 3.7 Parametric Study

Design of pipes without the internal pressure may change the design criteria, and since every gas pipeline carries pressurized gas in it, internal pressure can be a deciding factor for the designing of pipes. For this reason, we consider the internal pressure as a parameter to find the optimum pressure range to be used in a pipeline to get the maximum possible fault resistance. The design pressure for the pipe is calculated

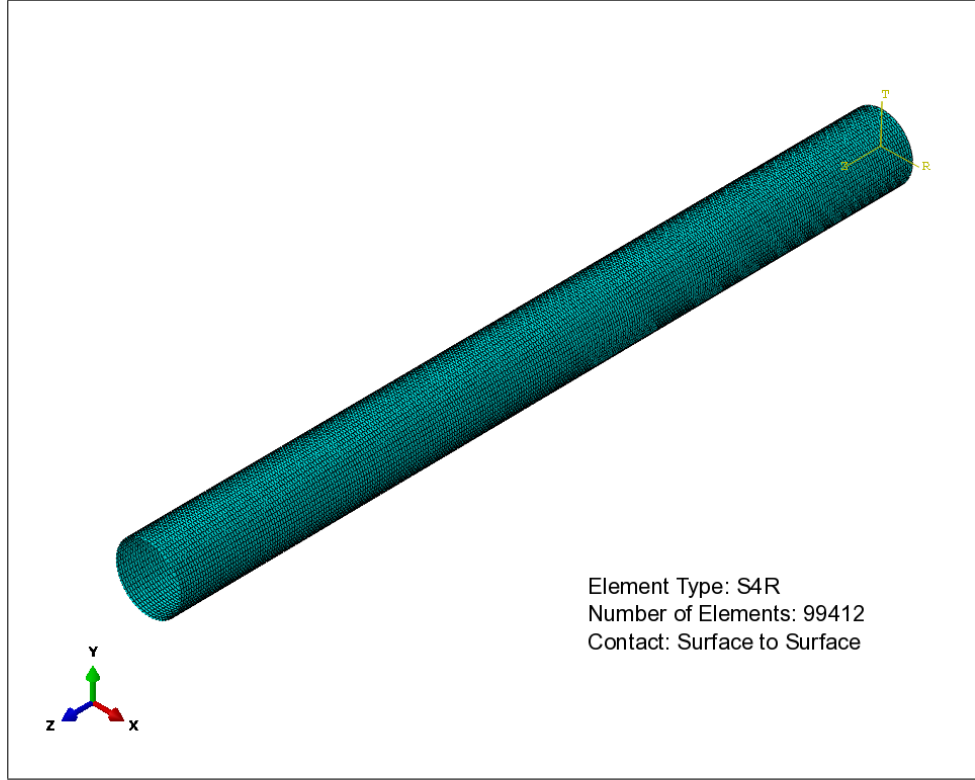


Figure 3.9: An example of the mesh used for the pipe model. The element type is the 4-node conventional shell element with reduced integration (S4R in ABAQUS).

using

$$P = \frac{2 \times 448 \times 0.0127}{914} \times 0.72 \times 1 \times 1 = 9MPa. \quad (3.4)$$

The required values, obtained from [1], are as follows:  $S= 448 MPa$ ,  $F=0.72$  and  $E=T=1$ .

Another interesting parameter to study is the standard dimension ratio, this parametric study gives the optimum diameter to thickness ratio for maximum fault resistance. This parameter will help to study the different failure patterns in thick and relatively thin pipelines.

The fault offset rate is another parameter considered in the present work. The present study will cover the effect of the fault-offset rate on the critical fault displacements due to peak ground velocities (PGV). The range of PGV values considered is

according to the average PGV value recorded in the earthquakes. The PGV will be attributed as fault offset rate in the rest of this study.

## CHAPTER 4: RESULTS AND DISCUSSIONS

### 4.1 Case I: Pipe Without the Soil

As explained in Chapter 3, the pressure load is applied in Case I to obtain buckling in the pipe. Figure 4.1 shows the deformed pipe shape and anticipated buckling. To observe the evolution of stresses and strains in the buckled area, we will analyze axial strains and axial stresses. The shell orientation is such that LE22 and S22 represents axial strain and axial stress respectively. Initially, the area near the fixed end experiences axial compression, which further evolves into the wavy structure shown in Figure 4.2. This wavy structure depicts the wrinkles in an actual pipe deformation. As the pipe continues to deform, one of the wrinkle dominates and strain increase suddenly resulting in shell mode of buckling, as shown in Figure 4.3.

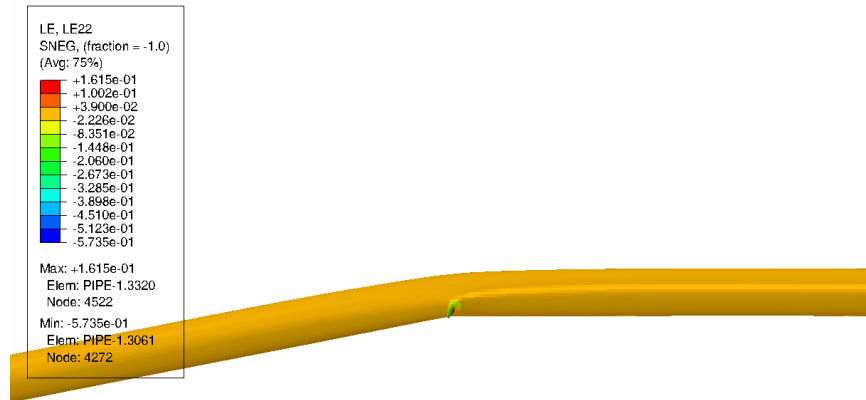


Figure 4.1: The contours represent the axial strains in the deformed pipe with buckling due to external pressure.

Figure 4.4 shows the evolution of axial strain in the buckled area. Here, X-axis

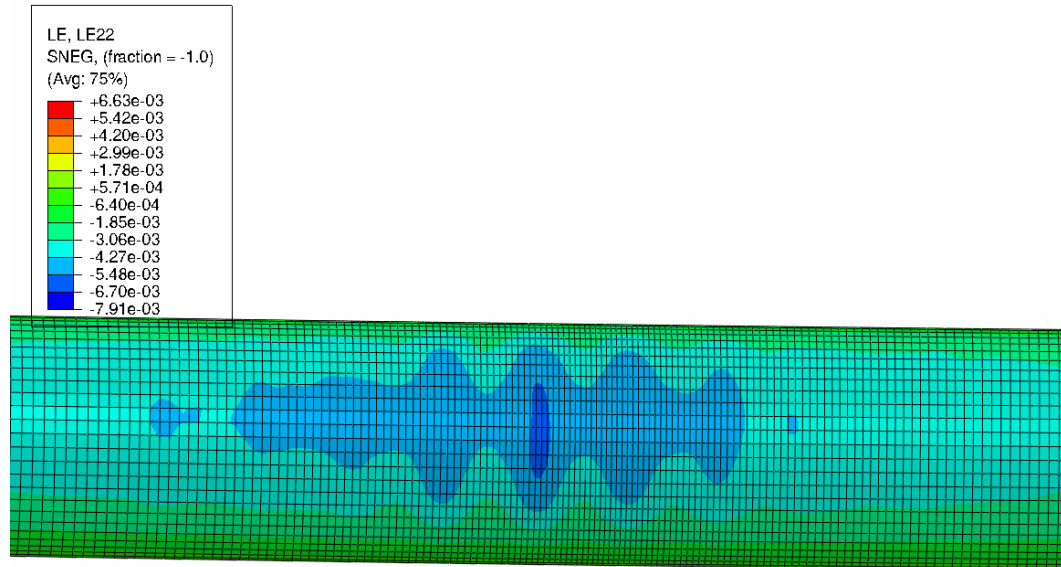


Figure 4.2: The contours represent axial strains before buckling in the pipe. The wavy pattern depicts wrinkling pattern in the shell mode of buckling.

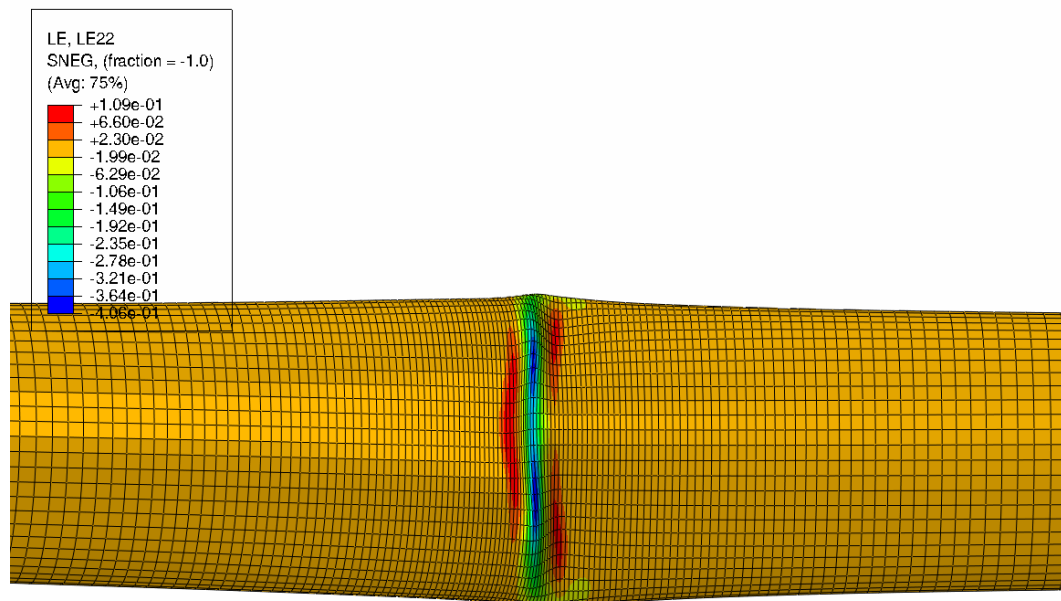


Figure 4.3: The contours represent axial strains after buckling in the pipe. The central region shows tension-compression-tension buckling failure.

represents 1.2 meters of pipe in the compressed region. The wavy structure is not very clear in this figure, so it will be explained in the next section in detail. The strain values are gradually increasing from time 0.2 seconds to 0.267 seconds. Strain shows a

sudden increase after 0.267 seconds, and the trend continues even beyond 0.3 seconds. This sudden rise in the strain makes it difficult to find the exact time when buckling starts. Figure 4.5 shows the time history of the axial stress of an element in the buckled region. The inner and the outer points are the integration points throughout the thickness of the shell element. Initially, the element is under axial compression. However, after 0.3 seconds the stress on the inner surface remains compressive while the outer surface experiences tensile stress. Hence, the outer and the inner surfaces of the same element are in tension and compression respectively.

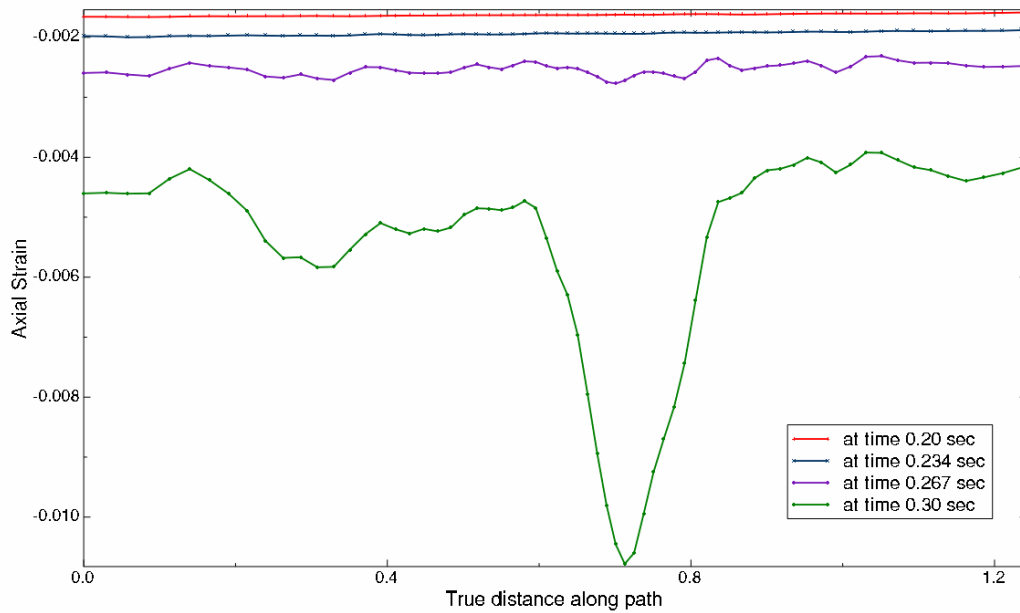


Figure 4.4: Evolution of axial strains in the buckled region of the pipe.

Figure 4.6 and Figure 4.5 show that the axial strain and axial stress for the same element exhibit similar behavior. The inner point is in compression and the outer point is in tension after 0.3 seconds. In sum, axial stresses and strains collectively conclude that onset of buckling occurs at 0.3 seconds.

Further, the study of the effect of different parameters on the pipe response is carried out. The parameters are as follows: mesh refinement, standard dimension ratio and internal pressure.

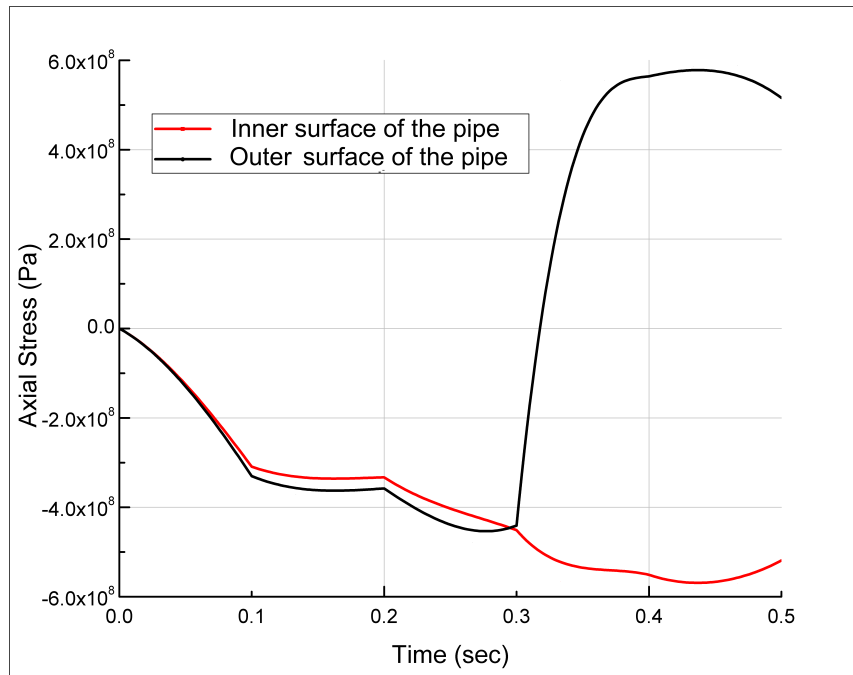


Figure 4.5: Axial stresses on the two integration points of the shell element in the buckled region of the pipe.

#### 4.1.1 Mesh Refinement

The mesh density is increased near the buckling region and the time of buckling and buckling patterns are recorded. Due to the drastic increase in strain after the onset of buckling, strains cannot be used for the convergence study. The buckling pattern shows no significant change after the second improvement in mesh as shown in Figure 4.7. And the onset of buckling occurs at 0.3 second in every case. This gives us the optimum mesh which will save the computational time and space for further studies.

#### 4.1.2 Standard Dimension Ratio

As discussed in Section 2.3, standard dimension ratio is the ratio of outer diameter to the thickness of the pipe. The ratio is varied from 48 to 144 keeping the diameter of the pipe constant. Figure 4.8 concludes that the time of buckling reduces as the

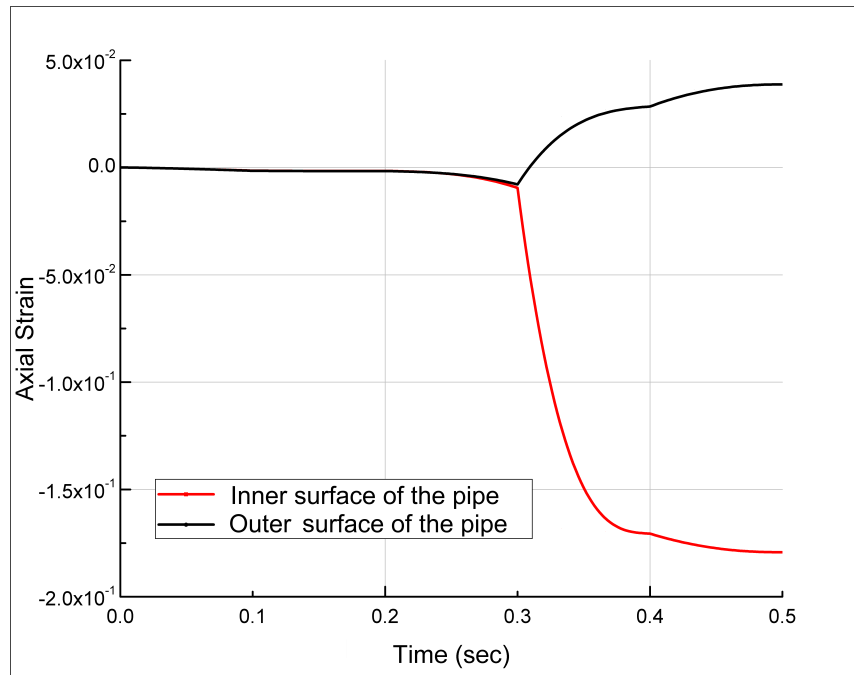


Figure 4.6: Axial strains on the two integration points of the shell element in the buckled region of the pipe.

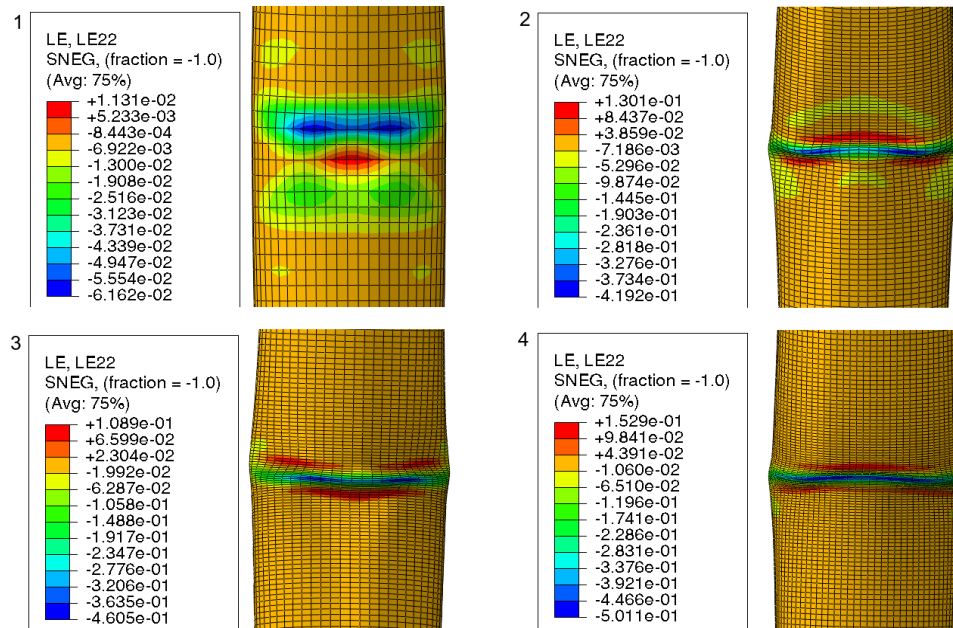


Figure 4.7: The contours represents axial strains in the pipe after buckling (at 0.3 seconds). 1,2,3 and 4 shows the increasing number of elements and the respective buckling patterns.

standard dimension ratio increases. In the initial increments of standard dimension ratio, time of buckling decreases rapidly, while in the case of thinner pipes the change in time of buckling is not very significant. In other words, buckling occurs sooner as the pipe gets thinner, and this is in accordance with the literature studied.

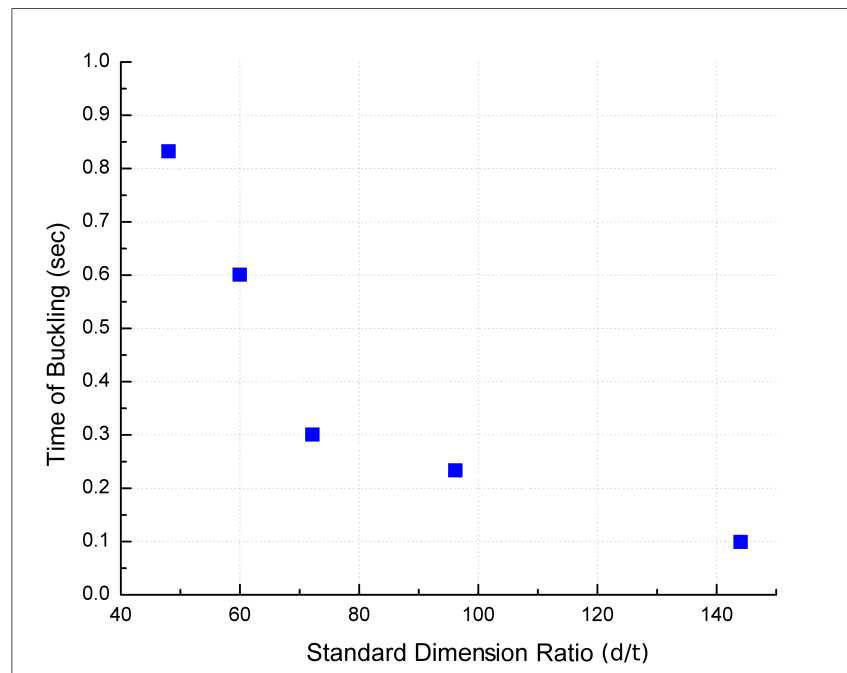


Figure 4.8: Standard dimension ratio vs time of buckling.

#### 4.1.3 Internal Pressure

The internal pressure of the pipe is varied from 0 MPa to 9 MPa which is its design pressure. The diameter of the specific wrinkled area increases significantly and can lead to rupture. The buckling pattern observed in all the pressurized pipes shows a bulge as seen in Figure 4.9. The time of buckling is recorded for different pressure values and plotted in Figure 4.10. From this plot we observe that the time of buckling changes by 0.1 seconds until 75% of its design pressure. Also, the pipe shows least fault resistance at its design pressure.

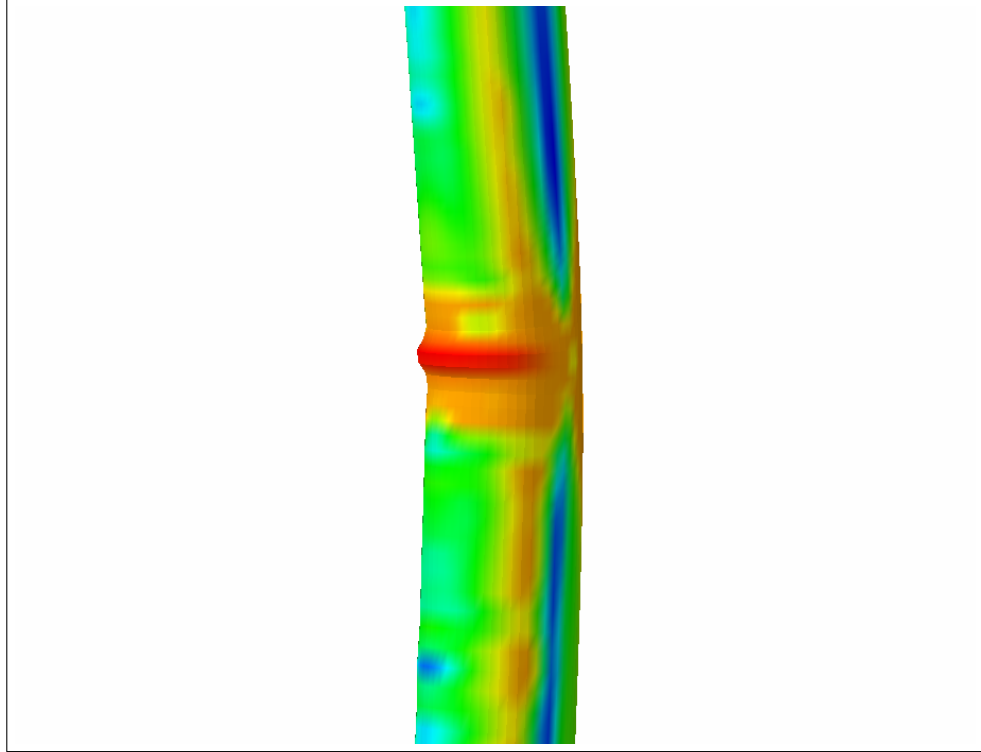


Figure 4.9: bulging shape buckling in a pipe with an internal pressure.

#### 4.2 Case II: Pipe-Soil Model

Figure 4.11 shows the deformed pipe-soil model. In this figure, U1 shows the nodal displacements in the positive X-direction, and its maximum value is essentially the fault displacement applied on the left block. The small green region between the red and the blue block is the fault slip width block and it contains fault plane. Figure 4.12 shows the anti-symmetrically deformed shape of the pipe. The inset shows the close view of the deformation in the pipe. Region A and B are the local buckling region in the stationary and moving block respectively, while at points C and D, pipe undergoes tension. Interestingly, at the fault plane, no significant deformation is observed. However, there is an insignificant ovalization observed at the fault plane at higher fault displacements.

The evolution of buckling shows similar pattern as observed in case I, Figure 4.13(a) shows a wavy pattern of strains before buckling and Figure (b) shows a localized buckle

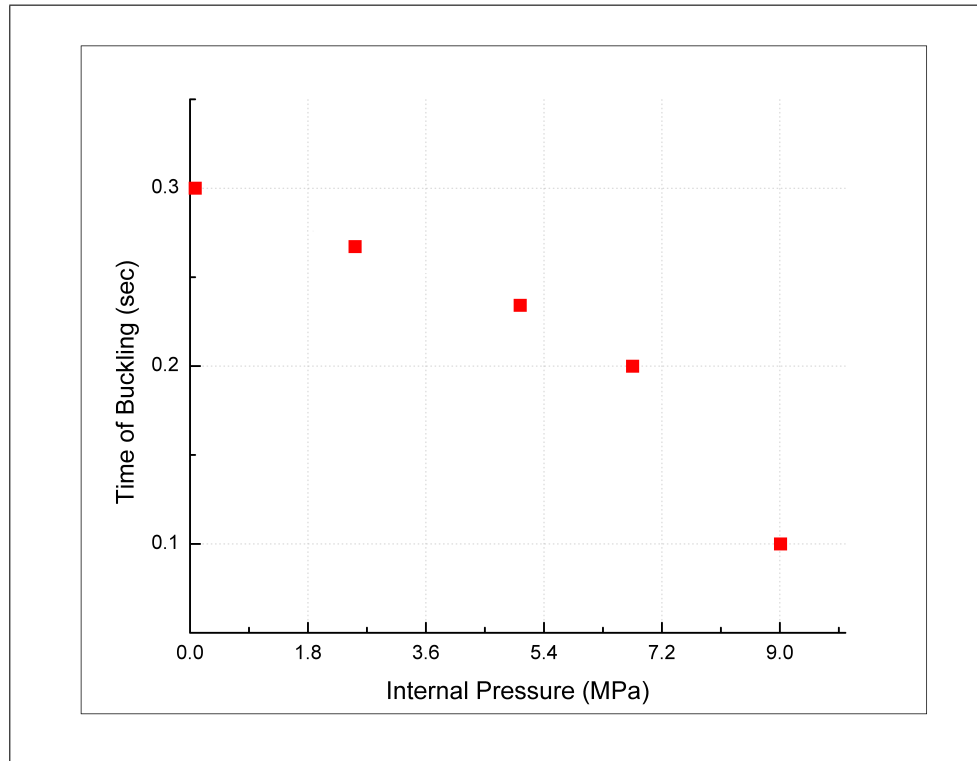


Figure 4.10: Effect of internal pressure on time of buckling.

in the pipe. In this case, one of the wrinkle dominates and forms a local kink in the pipe. According to ASME, no sharp kinks are allowed on the gas pipeline and need to be repaired immediately. Figure 4.14 shows the steady initial pattern until fault displacement of 0.4 m. Later, the wavy pattern is observed till 0.8 m and after that the strains evolve significantly. The waves are concentrated in the region where buckling occurs later, and the plot is almost symmetric about the failure point. Hence the formation of these wrinkles could upfront inform about the position of buckling in case of active faults. Moreover, the fact that buckling occurs at a distance from the fault plane, it is important to study the length between the two failure points. In this case, length between the two failure points is 10.6 meters, hence, at least 10.6 meters of the pipe has to be replaced or repaired.

In the previous case, we observed the time at which onset of buckling occurs which defined the failure criteria. In this case, the time of onset of buckling is used to

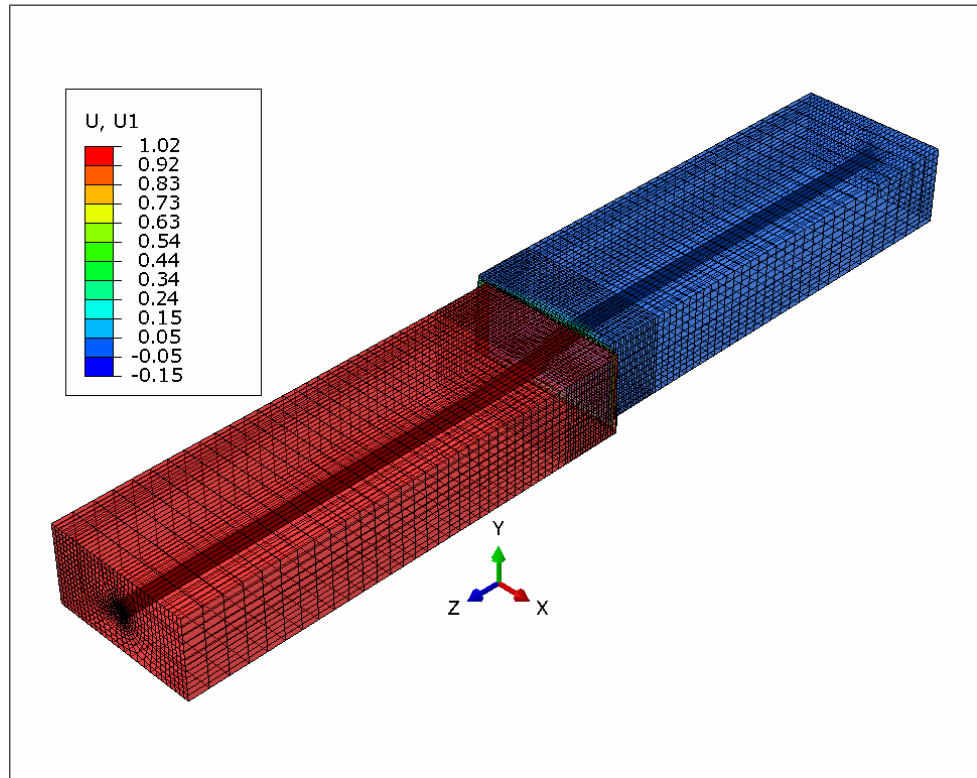


Figure 4.11: Deformation of the pipe-soil system. The contour colors represent the displacement component (in meters) in X-direction.

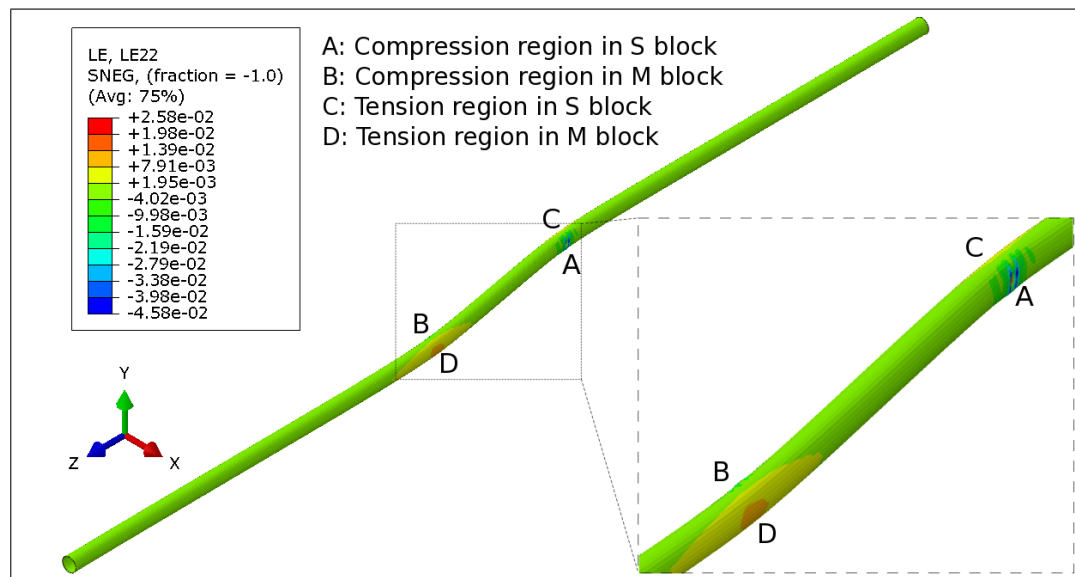


Figure 4.12: Anti-symmetrically deformed pipe with an inset showing the deformed regions. The contour colors represent axial strains.

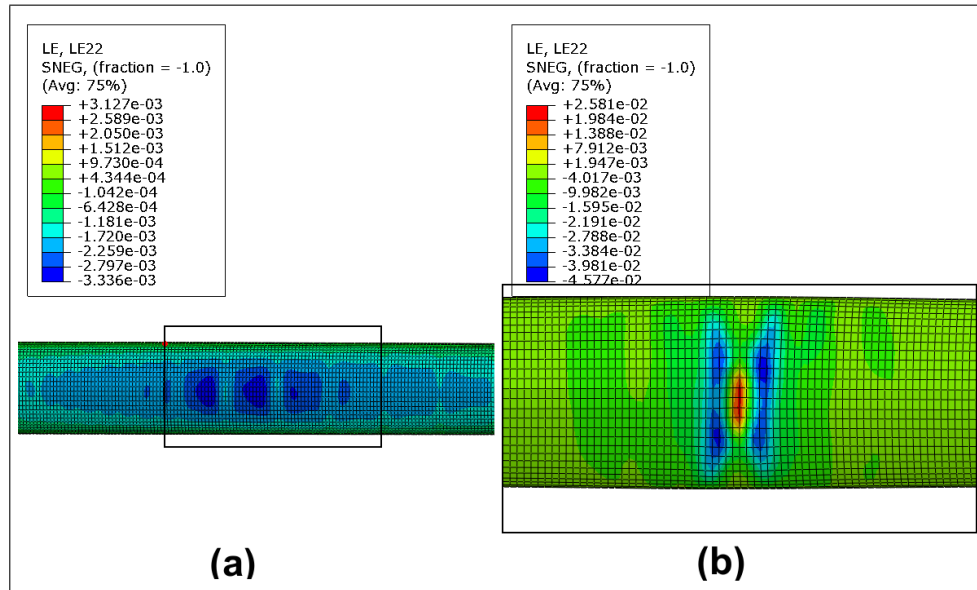


Figure 4.13: The contours represent axial strains in the pipe; a) Wrinkling pattern before buckling, b) Shell mode buckling.

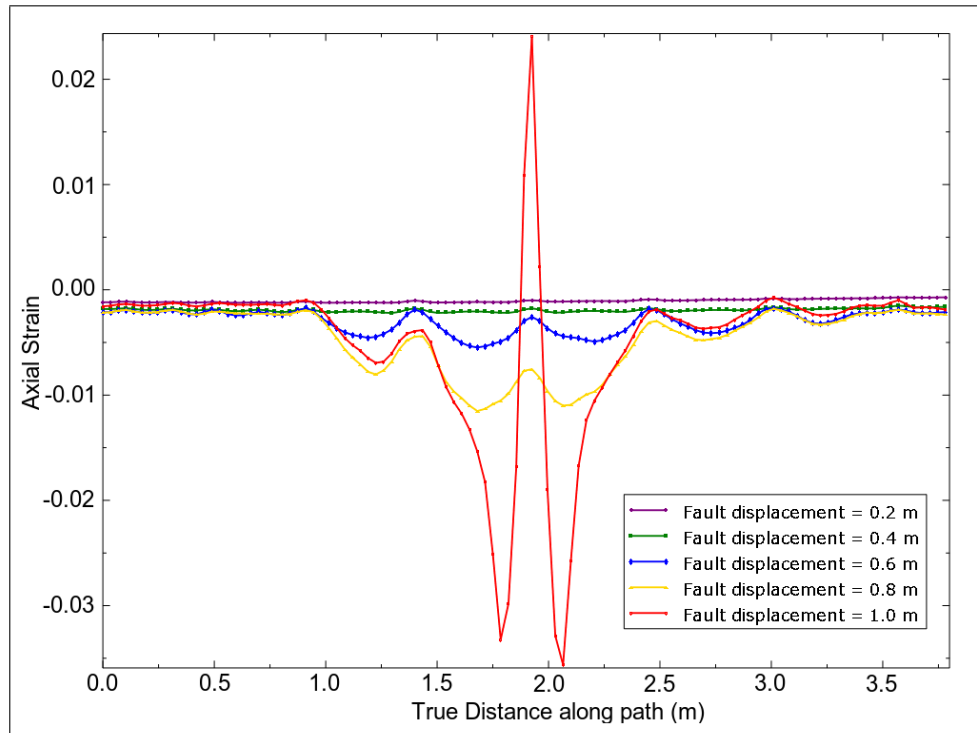


Figure 4.14: Evolution of axial strains in a buckled region of the stationary block.

find the applied fault displacement at that particular time. Then, the applied fault displacement at which pipe buckles is called as critical fault displacement. Therefore,

failure criteria for case II can be defined in terms of critical fault displacement. Figure 4.15 and 4.16 show the time history of axial strain and axial stress at an element in region A. The inner surface of the shell experiences tension while the outer surface experiences compression, which is expected by looking at the buckling pattern. The bifurcation occurs at around 0.96 seconds and the applied fault displacement at this time is 0.962 meters. Therefore, the critical fault displacement of the pipe with  $d/t$  ratio of 72 is 0.96 meters. Figure 4.17 shows the hoop stress at point A, and explains that the outer and inner surfaces behave in an exactly opposite manner. These two curves show spikes at the onset of buckling and can be used to capture the local buckling.

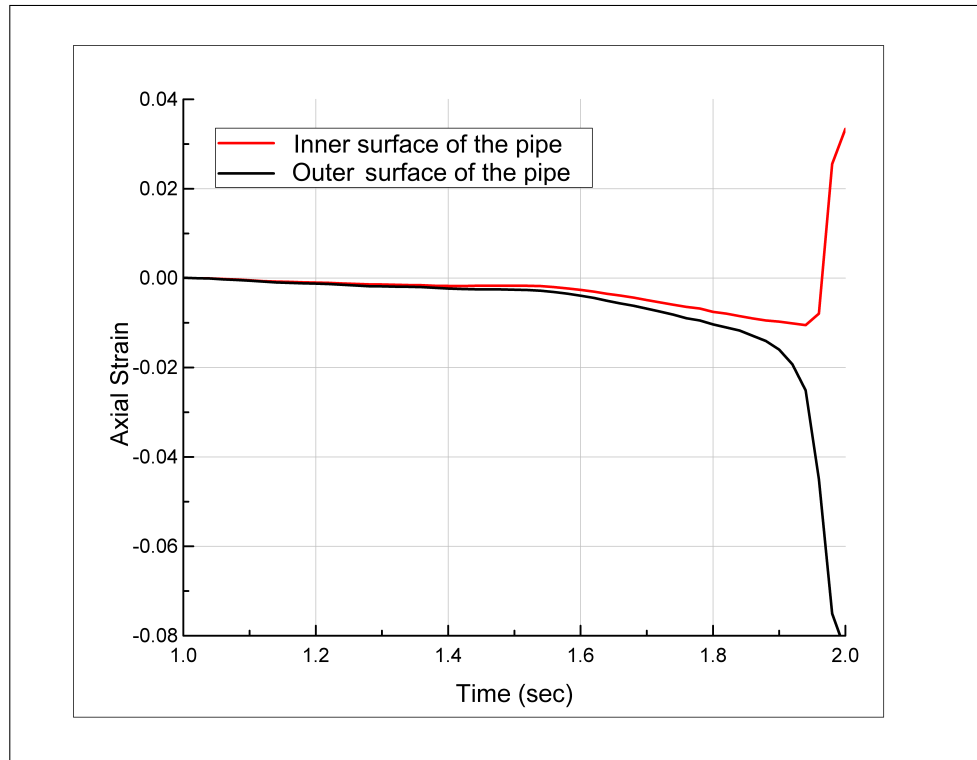


Figure 4.15: Time history of axial strains on the two integration points of the shell element in the pipe (region A).

On the opposite side of the buckled region, the pipe experiences tension in the region C, and the evolution of axial strain in this region is given by Figure 4.18. The systematic evolution of the axial strains does not increase significantly initially,

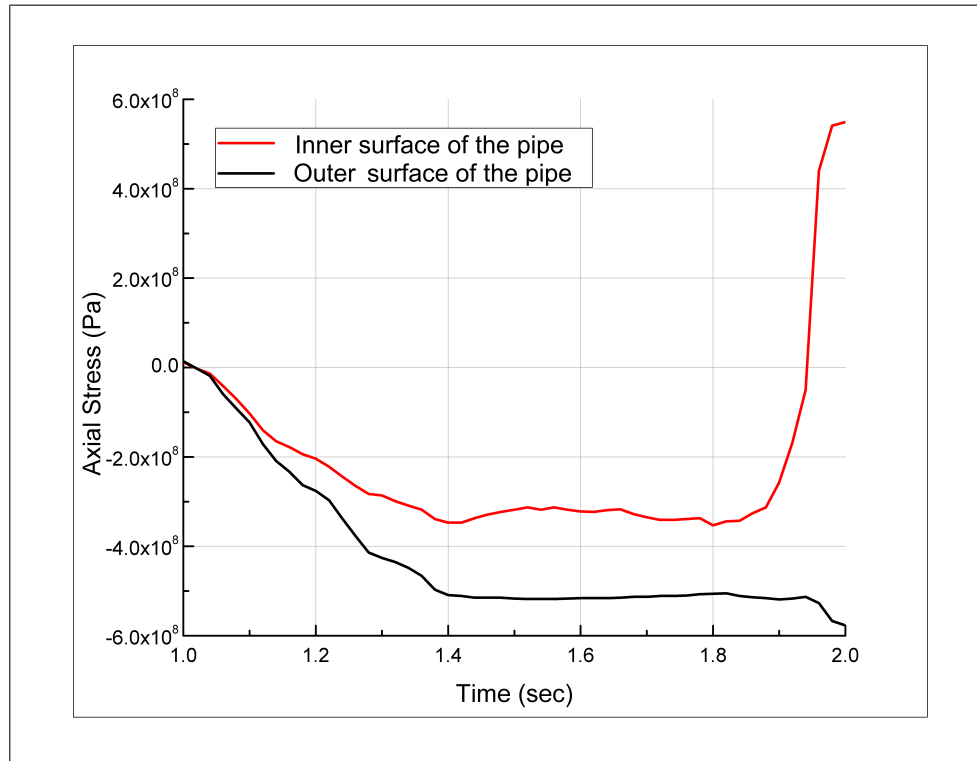


Figure 4.16: Time history of axial stresses on the two integration points of the shell element in the pipe (region A).

but after 0.4 meters to 1 meter it shows a sudden rise in the peak. However, these strain values are very less compared to the strain values in the buckled region. In post-buckling, these tensile stresses increases and it may cause tensile mode failure.

As explained in the numerical modeling, mass scaling is used in this study to save the computational expenses. The mass scaling factor used is 50 and Table 4.1 compare the results with simulation without mass scaling. The Mises stress is compared at the end of the gravity step, since no scaling is used in the second step. And the percentage error in the Mises stress is 2.4% and scaling does not change the critical fault displacement of the pipe.

Further, similar parametric study is carried out as of case I. In case II, the parameters being studied are as follows: mesh refinement, standard dimension ratio, fault offset rate, and internal pressure.

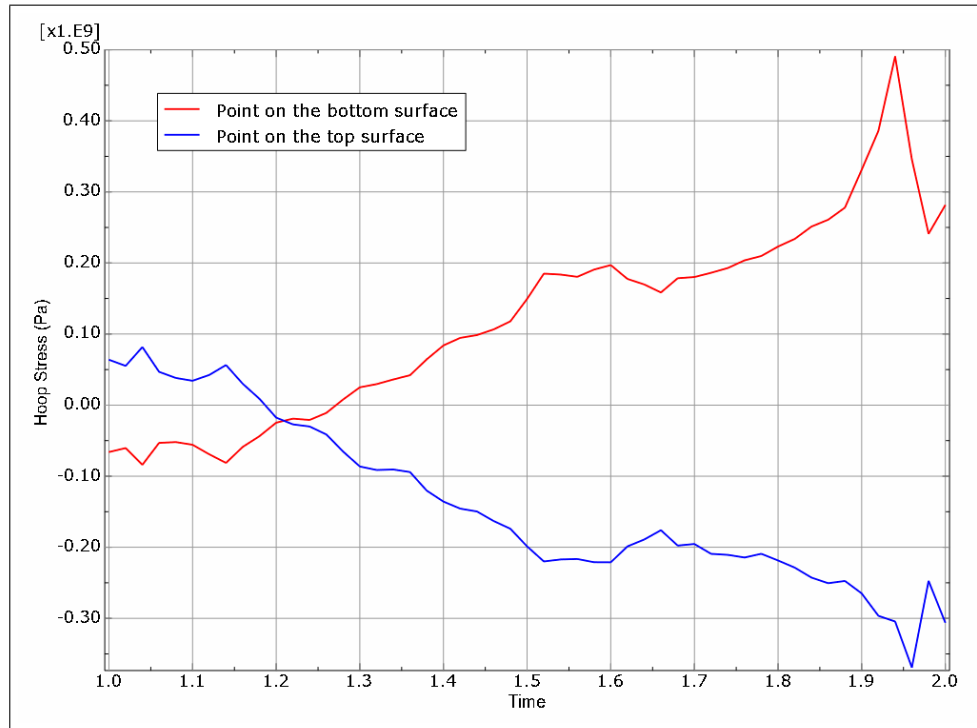


Figure 4.17: Time history of hoop stresses on the two integration points of the shell element in the pipe (region A).

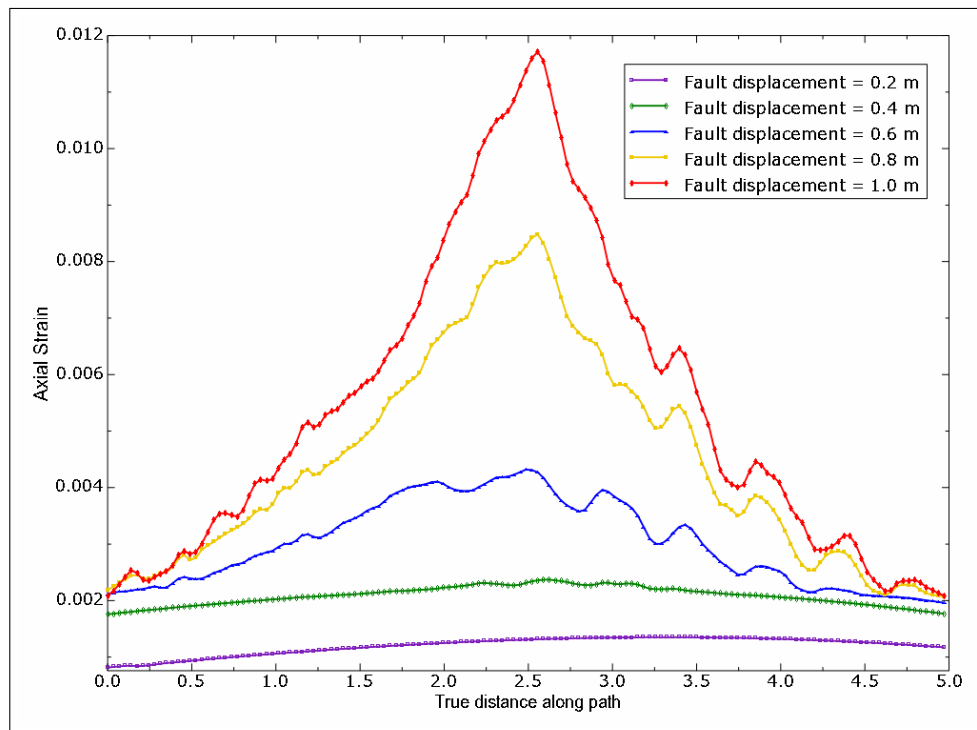


Figure 4.18: Evolution of axial strains in a tension region of the stationary block.

Table 4.1: Comparison of results with and without mass scaling.

Case	Mises Stress at the End of Gravity Step	Critical Fault Displacement
Mass Scaling	88.3 MPa	0.96 m
No Scaling	86.2 MPa	0.96 m

#### 4.2.1 Mesh Refinement

Keeping the elements in the angular direction of the pipe as a reference, mesh of the whole domain is refined. The three cases shown in Table 4.2 explains that the critical fault displacement does not change after case b. Keeping in mind that the mesh for soil block also need to be changed with the pipe and cost associated with the increasing number of elements, we proceed with case b. Figure 4.19 shows different buckling pattern formed due to three different mesh sizes. Here, ‘case a’ shows a completely different buckling pattern while ‘case b’ and ‘case c’ shows a similar pattern, a sharp kink. This again bolster the previous decision of proceeding with ‘case b’.

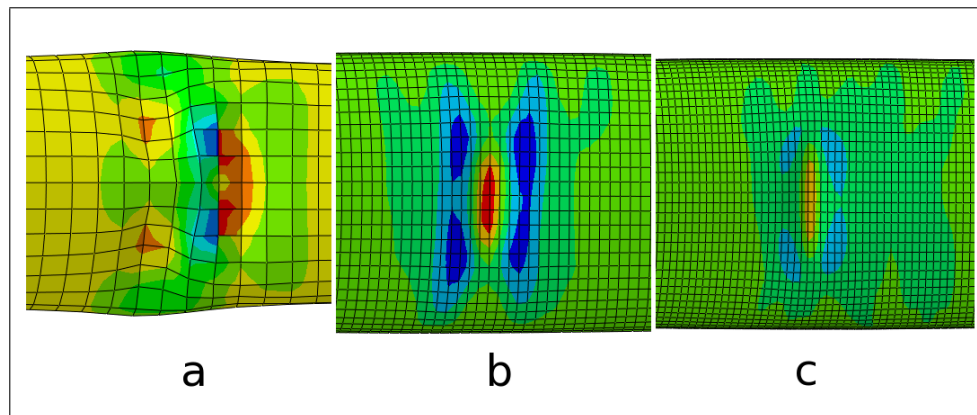


Figure 4.19: Different mesh refinements in the pipe and respective buckling patterns.

#### 4.2.2 Standard Dimension Ratio

Similar to case I, in case II, the standard dimension ratio is varied from 48 to 144. The fault displacement is applied on the soil until the buckling is observed in the pipe.

Table 4.2: Effect of mesh refinement on the pipe response.

Case	Circumferential Element in the Pipe	Total no of Elements	Max. Strain Before Buckling	Axial Displacement (m)	Critical Fault Displacement (m)
a	28	78103	-0.0139		0.675
b	59	162307	-0.0167		0.96
c	80	339050	-0.0170		0.96

The critical fault displacement is recorded and plotted against the standard dimension ratio, as shown in Figure 4.20. This plot shows that the critical fault displacement decrease as the standard dimension ratio increases. This clearly states that thicker pipes behaves better in the fault movement. In case of thinner pipe, pipe buckles in a diamond shaped buckling pattern as shown in Figure 4.21. This pattern agrees with the pattern shown by the experiments done by kyriakides [32]. Moreover, if the fault is applied after buckling has occurred, pipe folding is observed and tensile stresses generated by then may lead to rupture in the pipe. Furthermore, the distance between the two failure points changes with the dimension ratio. For thinner pipes the distance between the two failure points is approximately 8 m and for thicker pipes it is around 10 m.

#### 4.2.3 Fault Offset Rate

In this study, the effect of peak ground velocity on the critical fault displacement is investigated. To vary the peak ground velocity, time of displacement step is varied, and velocity range obtained is 0.33 m/s to 4m/s. In the reviewed literature, there is a very less or no study done on this parameter. The results are shown in Figure 4.22 which explains that the critical fault displacement increases with the increase in peak fault offset rate. The variation in the critical fault displacement is significant as the peak ground velocity increases, and the trend clearly states that the pipe will resist

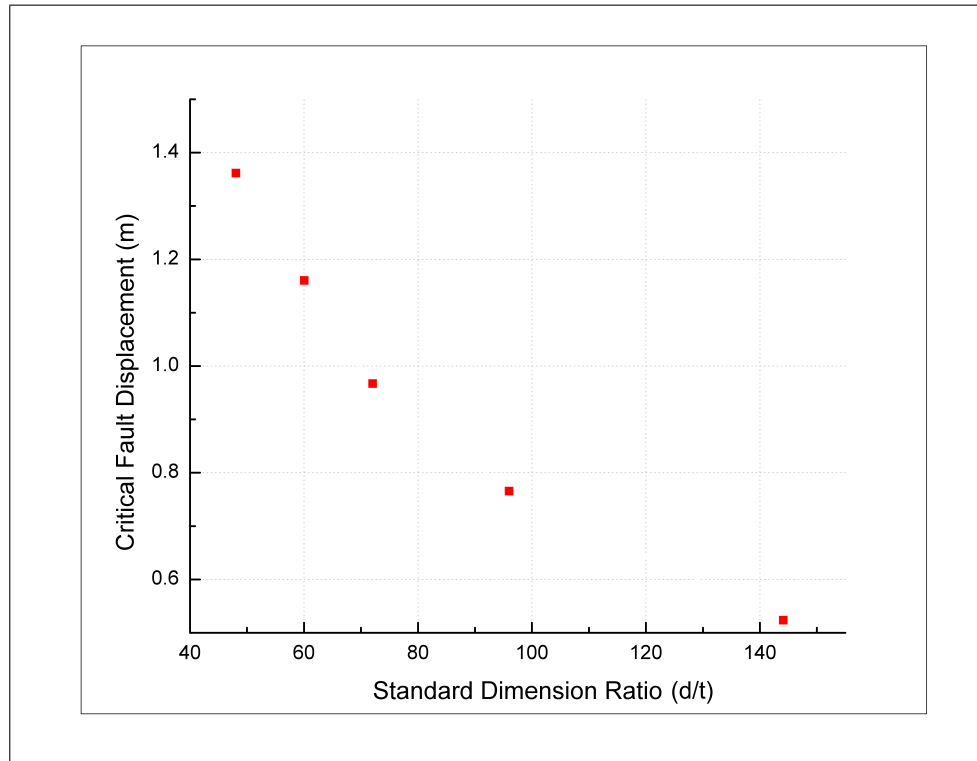


Figure 4.20: Effect of standard dimension ratio on the critical fault displacement.

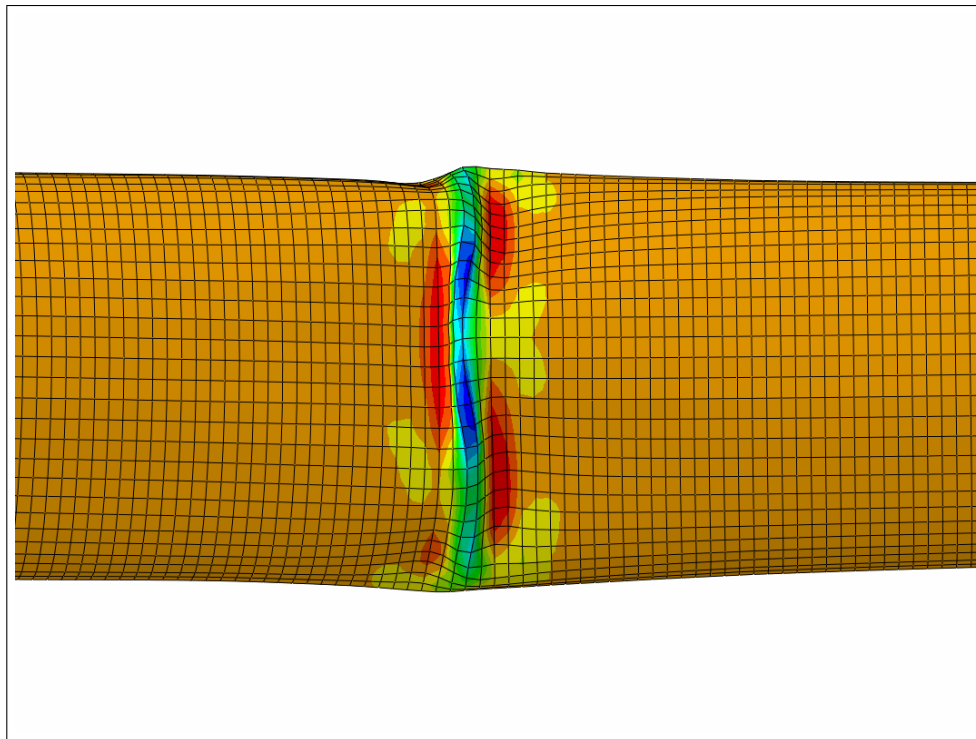


Figure 4.21: A diamond shaped buckling.

more as the fault offset rate increases. However, Figure 4.23 states that the time of buckling decreases as the fault offset rate increases. Due to rate sensitivity, the pipe can sustain larger displacements in higher fault offset rates.

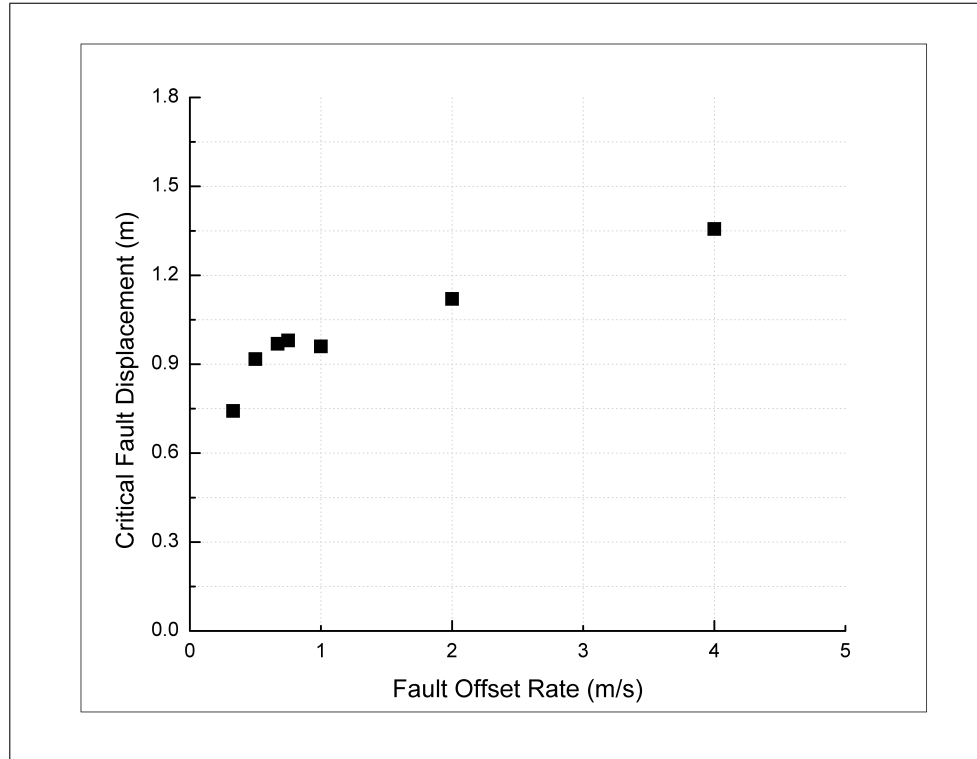


Figure 4.22: Effect of fault offset rate on critical fault displacement.

#### 4.2.4 Internal Pressure

Study of pressurized pipe serves the practical purpose of this study. Figure 4.24 shows the buckled shape of a pipe with an internal pressure and it matches closely with buckling pattern shown in the Case I. Actually buckled pipes due to ground motions confirm this bulging shaped buckling. The effect of the change in internal pressure on the critical fault displacement is shown in Figure 4.25 and the graph shows that for the design pressure (9 MPa) pipe has the least fault resistance. Pipe shows higher fault resistance for lower internal pressures. And the design pressure limit is certainly overestimated by the ASME code B31.8. Therefore, a factor considering the ground motion is suggested to be added to the pressure design formula.

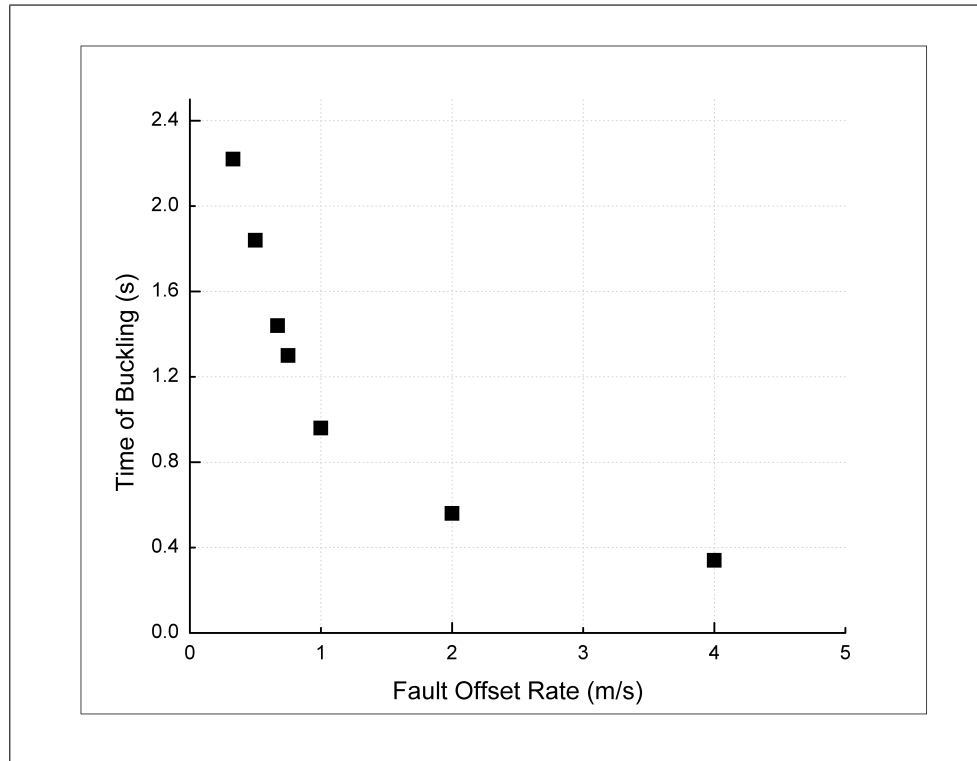


Figure 4.23: Effect of fault offset rate on the time of buckling.

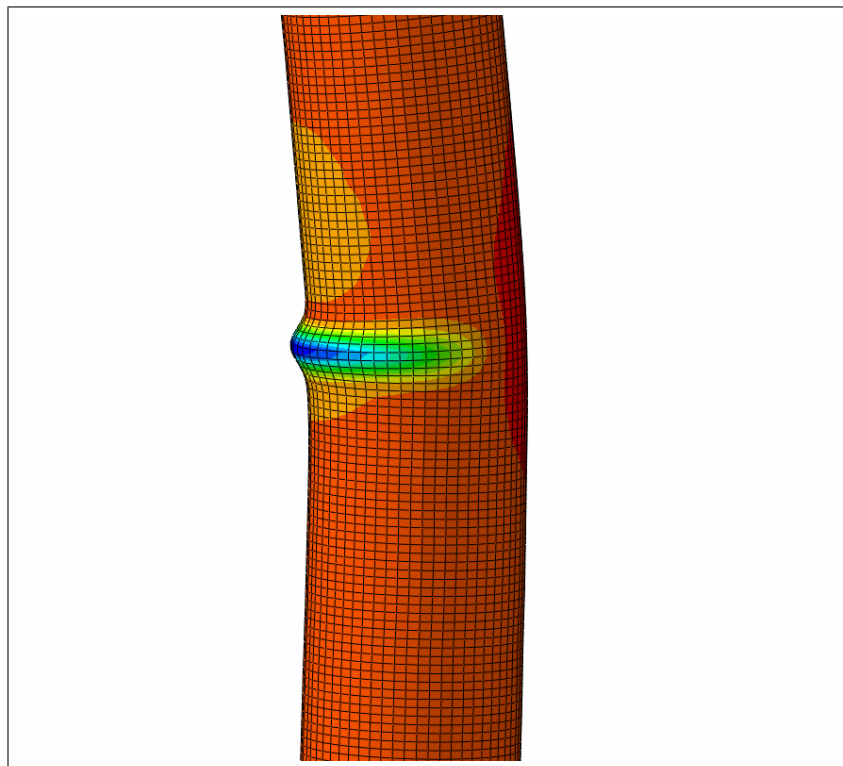


Figure 4.24: Buckling pattern in pipe with an internal pressure in a pipe-soil model.

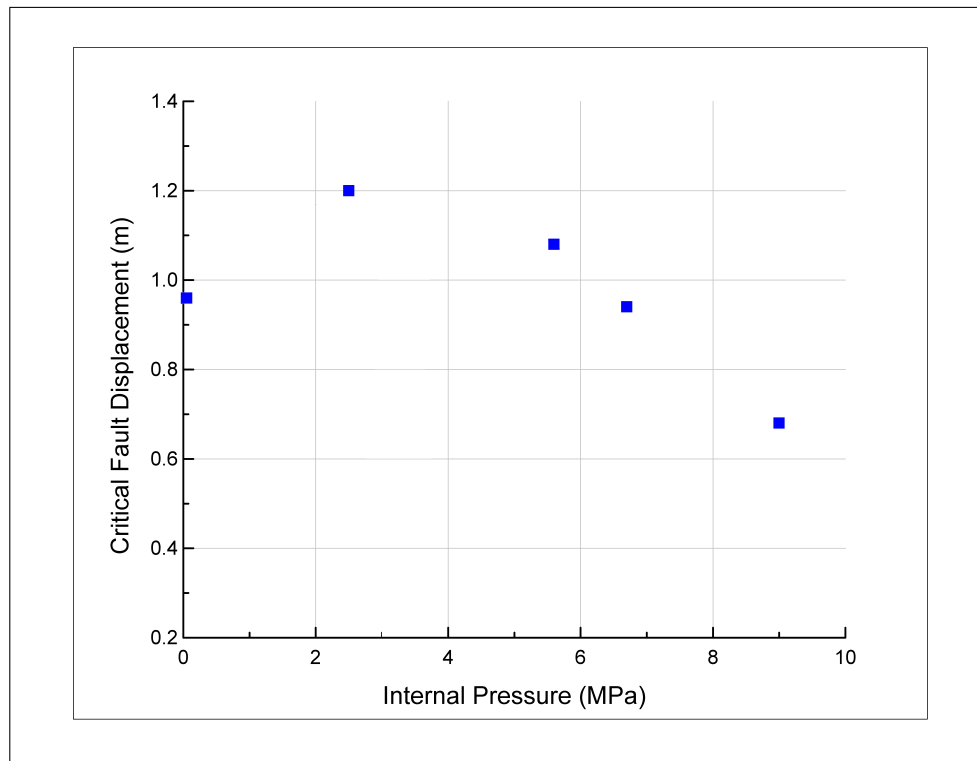


Figure 4.25: Effect of an internal pressure on the critical fault displacement.

## CHAPTER 5: SUMMARY AND CONCLUSIONS

In this work, the response of buried pipelines due to sudden ground movements was studied using the finite element method. The analyses were carried out using ABAQUS/EXPLICIT. The motivation behind this study was to understand the various parameters that affect pipe response and suggest ways to improve pipe design. A brief introduction to the geological faults and a literature survey was presented first. This was followed by the current guidelines for the design of buried pipelines. The analyses were carried out as two cases. First, only the pipe without the soil was considered to understand its response due to external and internal loads. In the second case, the pipe-soil assembly was modeled in the presence of a strike slip fault. In both the cases, buckling of pipes was taken to be the primary mode of failure and therefore, the focus was on studying the onset of buckling and buckling patterns as various parameters were varied.

The pipe model without the soil provided an insight into possible buckling patterns as the pipe was subjected to external and internal pressures. Furthermore, our studies of this model indicate that the mesh resolution is critical to predicting buckling pattern. However, the time of the onset of buckling does not require a very fine mesh. Furthermore, a parametric study was done on the following factors- standard dimension ratio, and internal pressure. The result shows that increase in the standard dimension ratio decreases the onset of buckling. In other words, thinner pipes are more prone to failure due to faults than thicker pipes which is in agreement with the previous published results. As the internal pressure increases, the fault resistance of the pipe decreases. The decrease in the fault resistance is not very significant below

the internal pressure of 67% of pipe's design pressure. After this, fault resistance decreases significantly until the design pressure of the pipe is reached.

The pipe-soil model provided the response of the steel pipeline due to sudden ground motion. Our results indicate that the pipe deforms always in an antisymmetric manner in a strike-slip fault. Pipes with faults crossing normally to it exhibit a localized buckling mode of failure. Unlike many of the previous studies, our study identifies the onset of buckling by observing sudden drops in strain and stresses.

A parametric study was carried out by varying standard dimension ratio, fault offset rate, and internal pressure individually. The standard dimension ratio showed results similar to those of case I. Different buckling patterns were observed for different cases. For high values of the standard dimension ratio, the pipes showed diamond shaped buckling while for lower values, a sharp kink was observed in the buckled region.

The effect of fault offset rate on the pipe was the most important study carried out in this thesis. There is a significant change in the critical fault displacement as the fault offset rate varies. Due to rate sensitivity, the pipe fault resistance increases with an increase in fault displacement. However, the time of buckling reduces as the fault offset rate increases. This collectively states that, although the pipe's fault carrying capacity increases in higher offset rates, the time required to achieve these fault displacements is less. Hence, pipe will buckle sooner with higher offset rates.

The third parametric study was done on internal pressure in the pipe. The results for the pipe without the soil case show that the time for the onset of buckling decreases monotonically as the internal pressure increases. Buckling mode of deformation is preceded by plastic deformation. In the case when the soil is present, the time for the onset of buckling increases initially and then decreases as the internal pressure increases. Thus, there is an optimal pressure for buckling resistance and beyond that the resistance decreases. This suggests a need to include a factor of safety for the optimum pressure range in the fault prone zones.

## 5.1 Recommendations for Future Work

The present study used several idealizations to carry out analyses. On the basis of that, this section will recommend further extension of this study. This study can be further extended by considering pipes under seabeds. This will be very helpful for analyzing the response of a submarine cable under the fault movement. The present study focused on the effect of a strike-slip fault. However, a normal fault or an oblique fault are also relevant since we know every strike-slip fault has a small normal and reverse fault components. Therefore, it will be more realistic to consider an oblique slip fault. In an actual practice, while installing a pipe, a backfill material is filled and the pipe is laid on it. Therefore, further study is suggested with the pipe laid on a backfill material surrounded by soil. This study assumed that pipe has failed as soon as buckling started but this is again a simplification. The recommendation for further study is to define different criteria such as safe operational levels, repairable failure levels and complete damage which would allow the operator to estimate the risk of failure.

## REFERENCES

- [1] American Society of Mechanical Engineers. Gas transmission and distribution piping system. ANSI/ASME 2014;B31:8.
- [2] Failure Investigation report -Tennessee GAS Pipeline 100-1 Rupture Batesville, MS. US Department of Transportation.
- [3] All Reported Pipeline Incidents- Listing by Cause. US DOT Pipeline and Hazardous Materials Safety Administration.
- [4] Weihao.chiu from zh [GFDL (<http://www.gnu.org/copyleft/fdl.html>) or CC-BY-SA-3.0 (<http://creativecommons.org/licenses/by-sa/3.0/>)], via Wikimedia Commons. Retrieved April 20, 2015.
- [5] By Ikluft (Own work) [GFDL (<http://www.gnu.org/copyleft/fdl.html>) or CC BY-SA 4.0-3.0-2.5-2.0-1.0 (<http://creativecommons.org/licenses/by-sa/4.0-3.0-2.5-2.0-1.0/>)], via Wikimedia Commons. Retrieved April 20, 2015.
- [6] <http://earthquake.usgs.gov/learn/topics/megaquakes.php>. Retrieved April 20, 2015.
- [7] <http://www.livescience.com/37052-types-of-faults.html>. Retrieved April 20, 2015.
- [8] [http://www.iris.edu/hq/programs/education\\_and\\_outreach/animations/2](http://www.iris.edu/hq/programs/education_and_outreach/animations/2). Retrieved April 20, 2015.
- [9] <http://www.artinaid.com/2013/04/components-and-types-of-geological-faults/>. Retrieved April 20, 2015.
- [10] <http://www.ei.lehigh.edu/learners/tectonics/faults/faults1.html>. Retrieved April 20, 2015.
- [11] [http://commons.wikimedia.org/wiki/File%3AOblique\\_slip\\_fault.jpg](http://commons.wikimedia.org/wiki/File%3AOblique_slip_fault.jpg). Retrieved April 20, 2015.
- [12] Bizzarri, Andrea. "Rupture speed and slip velocity: What can we learn from simulated earthquakes?." *Earth and Planetary Science Letters* 317 (2012): 196-203.
- [13] [http://www.seismo.ethz.ch/edu/FAQ/index\\_EN/#pgv](http://www.seismo.ethz.ch/edu/FAQ/index_EN/#pgv)
- [14] McGarr, A., & Fletcher, J. B. (2007). Near-fault peak ground velocity from earthquake and laboratory data. *Bulletin of the Seismological Society of America*, 97(5), 1502-1510.
- [15] MaCaffrey MA, ORourke TD. Buried pipeline response to reverse faulting during the 1971 San Fernando Earthquake. ASME, PVP conference 1983;77:1519.

- [16] Newmark NM, Hall WJ. Pipeline design to resist large fault displacement. In: Proceedings of U.S. national conference on earthquake engineering, 1975. p. 41625.
- [17] Kennedy RP, Chow AW, Williamson RA. Fault movement effects on buried oil pipeline. *ASCE Journal of Transportation Engineering* 1977;103:61733.
- [18] Wang LRL, Yeh YA. A refined seismic analysis and design of buried pipeline for fault movement. *Earthquake Engineering and Structural Dynamics* 1985;13:7596.
- [19] Wang, L. L. R., & Wang, L. J. (1995). Parametric study of buried pipelines due to large fault movement. *ASCE, TCLEE*, 6, 152-159.
- [20] Takada, S., Hassani, N., & Fukuda, K. (2001). A new proposal for simplified design of buried steel pipes crossing active faults. *Earthquake engineering & structural dynamics*, 30(8), 1243-1257.
- [21] Karamitros, D. K., Bouckovalas, G. D., & Kouretzis, G. P. (2007). Stress analysis of buried steel pipelines at strike-slip fault crossings. *Soil Dynamics and Earthquake Engineering*, 27(3), 200-211.
- [22] Liu, M., Wang, Y. Y., & Yu, Z. F. (2008, July). Response of pipelines under fault crossing. In Proceedings, international offshore and polar engineering conference, Vancouver, BC, Canada.
- [23] Nadukuru, S. S., Michalowski, R. L., Lynch, J. P., Green, R. A., Weiss, W. J., & Bradshaw, A. S. (2013). Finite Element Modeling of Buried Concrete Pipelines Subjected to Ground Rupture.
- [24] Abdoun, T. H., Ha, D., ORourke, M. J., Symans, M. D., ORourke, T. D., Palmer, M. C., & Stewart, H. E. (2009). Factors influencing the behavior of buried pipelines subjected to earthquake faulting. *Soil Dynamics and Earthquake Engineering*, 29(3), 415-427.
- [25] Ha, D., Abdoun, T. H., O'Rourke, M. J., Symans, M. D., O'Rourke, T. D., Palmer, M. C., & Stewart, H. E. (2008). Buried high-density polyethylene pipelines subjected to normal and strike-slip faulting-a centrifuge investigation. *Canadian Geotechnical Journal*, 45(12), 1733-1742.
- [26] Ha, D., Abdoun, T. H., ORourke, M. J., Symans, M. D., ORourke, T. D., Palmer, M. C., & Stewart, H. E. (2008). Centrifuge modeling of earthquake effects on buried high-density polyethylene (HDPE) pipelines crossing fault zones. *Journal of geotechnical and geoenvironmental engineering*, 134(10), 1501-1515.
- [27] Vazouras, P., Karamanos, S. A., & Dakoulas, P. (2010). Finite element analysis of buried steel pipelines under strike-slip fault displacements. *Soil Dynamics and Earthquake Engineering*, 30(11), 1361-1376.

- [28] Vazouras, P., Karamanos, S. A., & Dakoulas, P. (2012). Mechanical behavior of buried steel pipes crossing active strike-slip faults. *Soil Dynamics and Earthquake Engineering*, 41, 164-180.
- [29] Liang, J., & Sun, S. (2000). Site effects on seismic behavior of pipelines: a review. *Journal of pressure vessel technology*, 122(4), 469-475.
- [30] Datta, T. K. (1999). Seismic response of buried pipelines: a state-of-the-art review. *Nuclear engineering and design*, 192(2), 271-284.
- [31] ORourke, T. D., Jezerski, J. M., Olson, N. A., Bonneau, A. L., Palmer, M. C., Stewart, H. E., ... & Abdoun, T. (2008). Geotechnics of pipeline system response to earthquakes. *Geotechnical Earthquake Engineering and Soil Dynamics IV (GEESD)*, Sacramento, CA, May.
- [32] Kyriakides, S., & Corona, E. (2007). *Mechanics of offshore pipelines: volume 1 buckling and collapse (Vol. 1)*. Elsevier.
- [33] [http://www.doitpoms.ac.uk/tlplib/metal-forming-1/yield\\_non\\_metals.php](http://www.doitpoms.ac.uk/tlplib/metal-forming-1/yield_non_metals.php). Retrieved April 20, 2015.
- [34] Manual, A. U. (2013). Version 6.13-2. Dassault Systmes Simulia Corp., Providence, Rhode Island, USA.